Wear properties of Ni addition to Nb-V micro alloyed PM steels in dry and corrosive environment

Mohamed Ahmed Ahssi [1], Harun Çuğ[1], Bekir Güney [2,*], Mehmet Akif Erden [3], and Mustafa Acarer[4]

[1] Department of Mechanical Engineering, Karabuk University, Karabuk 78050, Turkey; ahssimohamed@yahoo.com (M.A.M.A.); hcug@karabuk.edu.tr (H. Ç)
[2] Vocational School of Technical Sciences, Karamanoglu Mehmetbey University, 70200, Karaman, Turkey; guneyb@kmu.edu.tr (B. G)
[3] Department of Biomedical Engineering, Karabuk University, Karabuk 78050, Turkey; makiferden@karabuk.edu.tr (M. A. E)
[4] Department of Metallurgical and Materials Engineering, Selcuk University, Konya 42130, Turkey; macarer@selcuk.edu.tr (M. A)

***** Correspondence: guneyb@kmu.edu.tr; Tel.: +90-338-226-20-00

Mohamed Ahmed Ahssi (0000-0001-9123-7510), Harun Çuğ (0000-0002-6322-4269), Bekir Güney (0000-0001-9764-9313), Mehmet Akif Erden (0000-0003-1081-4713), Mustafa Acarer (0000-0003-2876-4881)

(Received 27 August 2025; Accepted 01 July 2026)

Abstracts

The present study examines the influence of nickel addition on the microstructural evolution, phase formation, hardness, and wear performance of Nb–V microalloyed powder metallurgy (PM) steels under both dry and corrosive sliding conditions. A series of Fe–C–Nb–V alloys containing 0–30 wt.% Ni were produced via powder metallurgy by compacting mixed powders under high pressure followed by sintering at 1400 °C in an argon atmosphere. The resulting materials were characterized using optical microscopy, scanning electron microscopy (SEM), energy-dispersive spectroscopy (EDS), X-ray diffraction (XRD), density measurements, and microhardness testing. Tribological performance was evaluated through reciprocating wear tests under applied loads of 15 and 30 N in dry and 3.5 wt.% NaCl environments. The results revealed that the combined addition of Nb and V promoted grain refinement through the formation of carbide and carbonitride precipitates, resulting in enhanced hardness and wear resistance compared with unalloyed steel. Nickel addition further modified the microstructure and phase constitution, leading to the formation of bainitic, martensitic, and austenitic regions depending on the Ni content. Wear resistance improved progressively with increasing nickel concentration up to 13 wt.%, where the optimum combination of hardness and tribological performance was obtained. The alloy containing 13 wt.% Ni exhibited the highest hardness and the lowest material loss under both testing environments. However, excessive nickel additions (>13 wt.%) promoted microstructural heterogeneity and increased porosity, causing a decline in hardness and wear resistance. XRD analyses confirmed the presence of carbide phases such as Fe_3C and NbC together with Fe-Ni intermetallic compounds, which contributed to the observed strengthening mechanisms. These findings demonstrate that a controlled nickel addition, in combination with Nb–V microalloying, provides an effective strategy for optimizing the microstructure and wear performance of PM steels intended for applications requiring enhanced durability in both dry and corrosive service conditions.

Keywords: *Micro alloyed steel; Powder metallurgy; Nickel addition; Microstructure; Wear properties; Dry and corrosive environments*

Introduction

Low alloy high strength steel has been widespread used for a long time due to its superior mechanical and cost-effective properties in various industries such as heavy engineering industries, automotive industries, healthcare, defense, energy etc. [1-5]. In addition, significant advantages such as reducing waste material in the production of low alloy steel, fast production process, improving material quality [6], saving energy and reducing environmental emissions [7] can be achieved.

Recently, low carbon micro alloy steels produced by different methods have emerged as an important material for achieving high strength [8]. Unlike traditional high strength steels, which are distinctively composed of ferrite and pearlite, low carbon micro alloyed steels can be engineered to present excellent endurance and formability via improved microstructural contrives [9].

Microalloying is a steel production technology that involves additive trace amounts of strong carbide-forming elements such as nickel (Ni), titanium (Ti), niobium (Nb), vanadium (V), and aluminum (Al). With this method, composite micro alloyed steels with excellent properties such as superior strength, ductility, weldability, corrosion resistance and toughness can be produced by shaping the microstructure in the desired shape using different strength-enhancing mechanisms and appropriate thermo-mechanical processes [10-13].

In microalloying, mechanisms such as grain refinement, dislocation blocking, and solid solution strengthening are the primary processes for increasing mechanical strength [14]. Thermo-mechanical processing, on the other hand, is the process in which basic materials are converted into high-quality components by simply heating and shaping [15]. In the thermo-mechanical control course, processing parameters like reheating temperature and last rolling temperature have substantial effects on the properties of the material [16, 17].

Vanadium and niobium are effective microalloying elements in Powder Metallurgy (PM) steels as they increase the recrystallization temperature [18-20], improve mechanical properties and microstructure [18, 21]. During microalloying thermomechanical processing, elements such as V and Nb form carbides, nitrides or carbonitrides, which precipitate in the iron matrix and interacting by dislocations, increasing mechanical features via precipitation hardening [22-25]. The types, sizes, morphologies and amounts of these precipitates directly affect the mechanical properties [26]. These elements form fine precipitates of vanadium carbide and vanadium nitride (VC, VN) that limit austenite grain growth during austenitization, leading to improved strength and ductility [18, 21, 27]. Hardening, which is created by the precipitation of elements such as carbide and nitride, is the preferred strengthening mechanism, especially in forged products. In this mechanism, the size, distribution and type of compounds formed by carbon and nitrogen and micro alloying elements are important [3]. Among these microalloying elements, V acts as an effective precipitation strengthening element at low temperatures due to its high solubility in austenite, although it is lowly soluble in ferrite [18, 27, 28]. Precipitation strengthening effect is increased in V alloying, while fine grain weakens the strengthening effect [29]. Unlike other microalloying elements, vanadium promotes ferrite formation [18].

Carbon-rich VCN forms at temperatures lower than 700 °C. Vanadium precipitates formed during or after the transformation occur with diameters smaller than 0.03 µm. VN can compose within the austenite phases of high carbon steels (0.4%), particularly those with high nitrogen content, and can refine grain size akin to NbC [18, 30-32]. Since vanadium composes precipitates and VN precipitates prevent grain coarsening, it can also improve the properties of the alloy such as microstructure, yield, tensile, toughness, hardness strength and formability [3, 33-35].

Niobium is a very effective element in forming carbides and nitrides. NbC prevents the recrystallization of austenite at around 1000 °C, causing the formation of ferrite grains. In order for NbC to completely go into a solution, it must be kept at a high reheating temperature of around 1300 °C for a sufficiently long time. In this way, fine particles precipitate and increase the yield strength [36]. NbC precipitates with an average size of 200 nm in austenite, while 20 nm precipitates can delay recrystallization. In addition, a 2 μm NbC precipitate prevents grain coarsening of austenite during normalization. Niobium, which does not precipitate in austenite, precipitates during ferrite transformation and increases strength [3]. Adding niobium to steels increases their strength and toughness through precipitation strengthening [3, 36, 37].

Nb shows high familiarity by C and N, facilitating the creation of Nb(C,N) carbonitrides that conduce to durability the steel matrix [38]. Addition of Nb to micro alloyed steel affects the solidification mechanism. For example, Nb-containing phases in steel during solidification support the formation of ferrite and bainite. Ferrite is effective in improving toughness and plasticity [39]. The increment in Nb ingredient in steel results in a decrease in grain measure, which in turn results in a decrease in dislocations [40]. This effect creates a grain boundary strengthening mechanism as it makes the movement between adjacent grains more difficult [41].

PM is an effective technique to produce small, functional, non-conformable, difficult-to-manufacture composite components with superior mechanical and tribological properties in an advantageous and economical manner [3, 42]. Micro alloyed steels from these composite classes are produced with PM, but studies in these areas have not yet reached sufficient maturity [43-45].

Nickel acts as an austenite stabilizer by contracting the ferrite region while expanding the austenite region into steel. Nickel increases resistance to corrosion and oxidation at high temperatures. Nickel's ability to increase toughness and strength is due to its ability to improve grain size. Increases in properties such as fracture resistance, hardness, critical cooling rate, and ductility depend on the amount used in conjunction with chromium. Elemental nickel has a lower diffusion coefficient than most elements and diffuses more slowly in iron [44, 45].
Adding too much Ni to the alloy increases the tendency to form granular bainite (GB) and martensite-austenite (MA). The ratio of high-angle grain boundaries in the GB structure is low and does not considerably hinder crack propagation, whereas MA constituents frequently lead to crack leads to crack induction and growth, thereby deteriorating the material's low-temperature toughness [45, 46]. Although it is reported that further addition of Ni will evolve the tensile strength, hardness, density and prevention of corrosion products [44, 45], various features of high density dislocation sites deteriorate the local corrosion resistance of micro alloyed steel [45, 46]. In particular, it significantly increases the micro-galvanic corrosion affect along grain boundaries, leading to fast resolution of the austenitic matrix [47].

Microalloying represents an effective approach for tailoring the mechanical performance of low-carbon steels through the incorporation of minor additions of alloying elements such as niobium (Nb), vanadium (V), and nickel (Ni). Among these elements, Nb and V are widely recognized for their ability to enhance strength by suppressing austenite grain growth, thereby promoting grain refinement, and by contributing to precipitation strengthening through the formation of fine carbonitride precipitates [48-50]. In addition to these strengthening mechanisms, nickel plays a crucial role in improving toughness and ductility. This effect is primarily attributed to its influence on the stacking fault energy of austenite, which modifies dislocation movement and deformation behavior during plastic straining [51].

In this study, steels with 8 different alloy compositions were manufactured by adding Ni element at different weight ratios to micro alloyed steel produced with PM technique. The focus of the study is the effect of Ni element on microstructure dry sliding and corrosive wear of micro alloyed steels.

Materials and Experimental Procedure

Steel samples with the necessary compositions are created using powder metallurgy in this investigation. In the investigation, we looked at how varying concentrations of Ni and micro-alloying components affected the microstructure and mechanical characteristics like wear resistance and hardness. The steel specimens were made using iron, graphite, niobium, vanadium, and nickel powders. Niobium (Nb) and vanadium (V) powders were supplied by Sigma-Aldrich (USA), while iron (Fe) and graphite powders were procured from Höganäs (Sweden), and nickel (Ni) powder was obtained from Nanografi (Türkiye). According to the manufacturers' specifications, the particle sizes of graphite, Fe, Nb, V, and Ni powders were below 20 µm, not exceeding 180 µm, below 45 µm, 44 µm, and below 5 µm, respectively. The corresponding purity levels were reported as 96.5%, 99.9%, 99.8%, 99.5%, and 99.7%.

Prior to mixing, the powders were weighed using a precision scale marked with the RADWAG AS-60-220 C/2 trademark at 104 g. The chemical makeup of the powders is shown in Table 1. Fe-C-NbV-xNi particles were mixed for one hour in a TURBULA T2F apparatus (Willy A. Bachofen AG, Muttenz, Switzerland) capable of three-dimensional motion. The prepared powders were shaped in a mold (32 mm x 10 mm) in the shape of the wear test specimen in a hydraulic press (Hidroliksan, Konya, Turkey) with a 100-ton capacity and 750 MPa press pressure. Sintering was carried out in an argon atmosphere furnace at 1400 °C for 2 hours. The densities of the samples were determined using the Radwag density kit (Bruker Alpha, Bursa, Turkey) according to the Archimedes principle in accordance with the ASTM B 328-96 standard [52]. Table 1 shows the alloy densities and chemical compositions of the samples coded S1-S8.

Optical images of the samples were obtained using a Nikon ECLIPSE L150 microscope (Melville, NY, USA). Grain sizes of the alloys were determined by the mean linear intercept method [53, 54]. Microstructure and fracture surface micrographs were obtained using a Zeiss microscope. To determine the phase composition and structure of the produced steels, X-ray diffraction (XRD) analysis was performed at the Karamanoğlu Mehmetbey University Scientific Research Center (KMU-BILTEM) using a Bruker Advance D8 model instrument. The structure and composition of the phases were identified using Panalytical HighScore Plus®, which utilizes the International Diffraction Data Center (ICDD) database. Microhardness of the samples was measured using a SHIMADZU hardness tester (MCT-W, Shimadzu, Tokyo, Japan).

Table 1. Chemical compositions of powder metal steels.

Samples	Compound	Mass spectrum (% wt)				
		Graphite	Nb	V	Ni	Fe
S1	Fe + C	0.55	-	-	-	rest
S2	Fe + C + 0.15 (Nb + V)	0.55	0.075	0.075	-	rest
S3	Fe + C + 0,15 (Nb + V) + 5Ni	0.55	0.075	0.075	5	rest
S4	Fe + C + 0.15 (Nb + V) + 10Ni	0.55	0.075	0.075	10	rest
S5	Fe + C + 0.15 (Nb + V) + 13Ni	0.55	0.075	0.075	13	rest
S6	Fe + C + 0.15 (Nb + V) + 15Ni	0.55	0.075	0.075	15	rest
S7	Fe + C + 0.15 (Nb + V) + 20Ni	0.55	0.075	0.075	20	rest
S8	Fe + C + 0.15 (Nb + V) + 30Ni	0.55	0.075	0.075	30	rest

The surfaces were prepared using a conventional sample preparation technique using 800 mesh sandpaper. Wear tests were carried out in two different environments, dry and abrasive, on a UTS-10 tribometer tester with a 10 mm reciprocating motion, as shown in Figure 1. A steel ball made of AISI 52100 (100Cr6) was used as the abrasive in the test device. The applied loads in the test procedure were 15 and 30 N, the total wear distance was 1000 meters, and the sliding speed was 50 rpm. After each wear test, the worn surfaces were cleaned with ethanol. Dry wear tests were carried out at room temperature in an open atmosphere. Distilled water, a 3.5% NaCl solution, was used to constitute 100 ml of the abrasive wear medium. At the end of each test, the solution added to the wear cell during abrasive wear was replaced. Wear weight losses were weighed using an electro balance with a precision of 0.0001 mg. The coefficient of friction and friction force were calculated using the wear device's software. Following the wear test, SEM images and EDS analyses of the worn surfaces were collected. The depth and cross-sectional area of the worn surfaces were examined using a surface profilometer.

Figure 1. Wear tester unit

3. RESULTS AND DISCUSSION

Microstructure and Wear Characteristics

The optical microstructures of steel samples produced by powder metallurgy technique sintering at 1400°C in an argon atmosphere are shown in Figure 2. The images clearly show that the unalloyed powder metallurgy steel consists of ferrite and pearlite phases. To improve the tensile and hardness strengths of the microalloyed steel, different amounts of alloying elements were added in Nb-V double and Nb-V-Ni triple combinations. It can be noted that with the addition of these alloying elements, the pearlite and ferrite phases are smaller and more localized. In this study, the addition of 0.15% Nb-V resulted in a reduction in grain size compared to the Fe-C alloy without Nb-V. This resulted in increased strength due to the precipitates formed. With the addition of 5% Ni, the presence of pearlitic and bainitic phases in the structure is observed. Furthermore, with the addition of 10% Ni, the bainitic and martensitic phases in the structure are seen to increase. When 13% and 15% Ni were added to the structure, it was observed that residual austenite was also present. Adding 20% and higher amounts of Ni to the structure resulted in an increase in the amount of residual austenite. This was considered a significant reason for the decrease in strength.

In line with the literature [56] during sintering and cooling, niobium and vanadium microalloy elements, confirmed by XRD analysis, precipitated as carbides, nitrides, and carbonitrides. This improved the mechanical properties of microalloy steel samples through mechanisms such as grain refinement, solid solution hardening, and precipitation hardening.

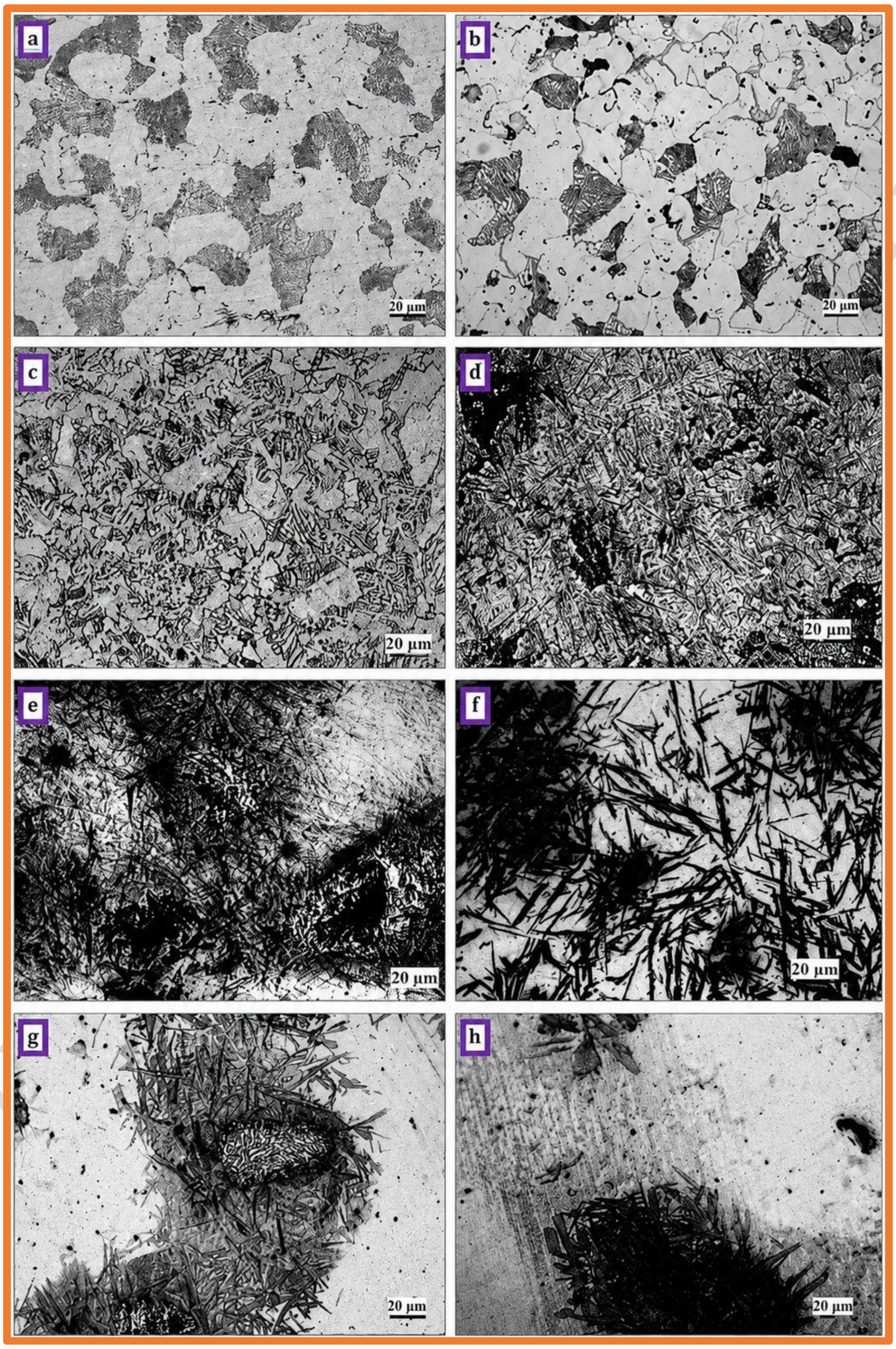

Figure 2. The optical micrographs of the alloys a) S1, b) S2, c) S3, d) S4, d) S5, e) S6, f) S7, g) S8

The values obtained from the wear amounts, friction coefficients, density and hardness measurements of the samples produced by adding Nb and V to TM unalloyed steel are presented in Table 2. The graphs of the wear amounts occurring under the influence of physical properties such as friction coefficient, hardness and density are given in Figure 3 and Figure 4. The lowest wear occurred in the corrosive wear environment of sample S5 at 15 N load, while the highest wear occurred in sample S1 at 30 N load in a dry sliding environment. According to the wear test results, the wear depth of PM steel specimens increased with the applied load. Despite having the same carbon content across all alloy compositions, a significant improvement in wear resistance and hardness was observed with the increased presence of Ni in the micro alloyed components. Additionally, an improvement in density was noted, attributed to the precipitation effects of the microalloying elements and the Ni content. Mechanisms such as grain size refinement and precipitation of microalloying elements are believed to be the primary contributors to the enhancement of mechanical properties.

Table 2. Wear, friction coefficient, density and hardness test results of TM steels sintered at 1400 °C.

Samples	Load in dry sliding (N)				Load in corrosive sliding (N)				Density (g/cm3) [55]	Hardness ($HV_{0.5}$) [55]
	15		30		15		30			
	Wear loss (mg)	Friction coefficient	Wear loss (mg)	Friction coefficient	Wear loss (mg)	Friction coefficient	Wear loss (mg)	Friction coefficient		
S1	24.255	0.0968	35.866	0.0980	3.568	0.0721	6.882	0.0649	7.2837	75
S2	13.466	0.0972	23.118	0.1086	2.776	0.0791	5.450	0.0638	7.2787	125
S3	9.430	0.0985	15.187	0.1043	2.388	0.0721	5.008	0.0898	7.4102	160
S4	4.558	0.0936	8.813	0.1098	1.504	0.0688	3.972	0.0746	7.2347	243
S5	2.734	0.1028	7.367	0.1164	1.344	0.0872	3.704	0.0897	7.5947	244
S6	3.912	0.1126	9.550	0.1187	1.596	0.0856	4.628	0.0862	7.6724	191
S7	5.908	0.1092	13.182	0.1182	2.188	0.0831	4.976	0.0844	7.6212	133
S8	8.804	0.0975	17.999	0.1019	2.608	0.0689	5.561	0.0555	7.2903	93

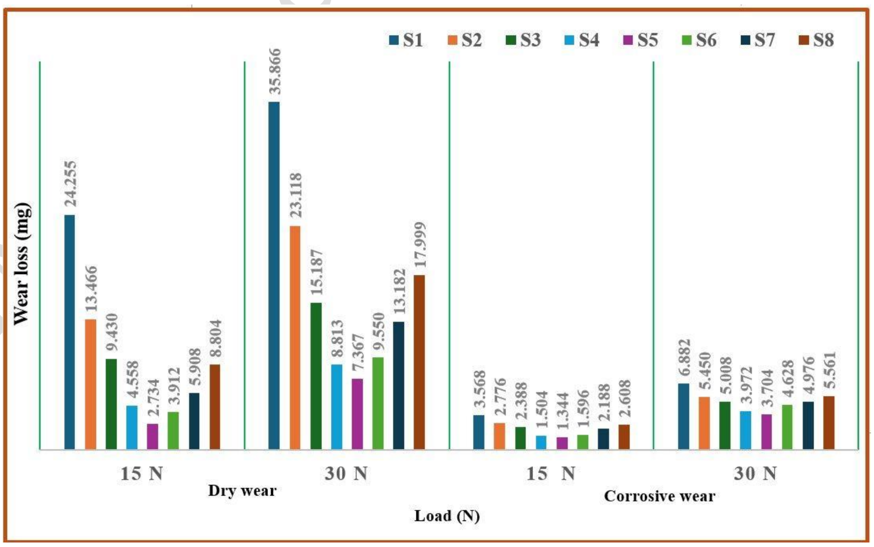

Figure 3. Weight wear amounts in dry sliding and corrosive sliding

Wear resistance and hardness can be improved in micro alloyed low carbon steel by TiC-VC precipitates. Also, carbides and nitrides in micro alloyed steel increment the hardness and durability of steel. It is accepted that the reason for the low rates of solid solution hardening is carbide and nitride precipitation [3, 57].

EDX analyses taken from the surfaces of samples abraded under 30 N load in dry and corrosive environments are shown in Figure 5 and Figure 6. The elemental structures and EDX peaks by weight of the samples typically reflect the chemical compositions of the samples.

Studies (Mishra et al., 2002) have demonstrated that the creation of carbides and nitrides in various compositions is caused by the presence of several microalloying elements in the alloy. These precipitates contribute significantly more actively to the increase in strength. The impact of solid melting hardening on the increment in strength diminishes as precipitates form because there is less carbon and nitrogen in the solid melt in free form [58]. Based on these results, and consistent with the XRD analyses and EDX results obtained within the scope of this study, it can be said that the formation of NbC, VC, and NbVC (N) precipitates (Nb-V) and carbide structures such as FeC, Fe_2C, Fe_3C, Fe_5C_2, and NbC in the structure of microalloyed TM steel is a significant reason for the increase in strength.

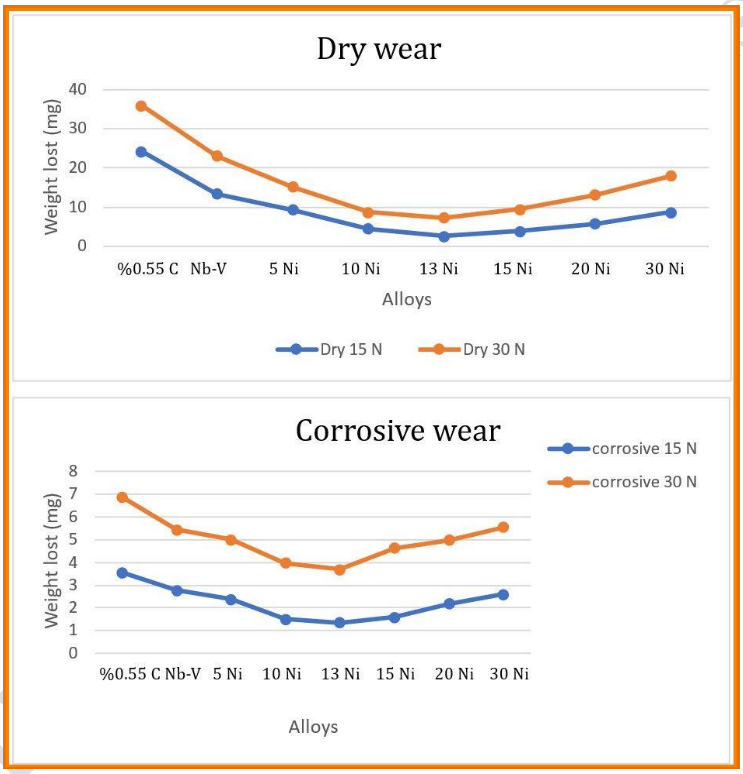

Figure 4. Weight loss graphs

Table 2 shows that as the (Nb-V) ratio increases, the wear resistance and hardness values increase. Consistent with previous studies [18, 56, 59], it is assumed that the distribution of precipitates of different sizes such as NbC (N), VC (N) in the matrix, and structures such as FeC, NbC cause this shift in strength values.

This could happen as a result of the formation of minute precipitates, like niobium carbonitride (NbCN) and vanadium carbonitride (VCN), either during the 1400 °C sintering process or the subsequent cooling phase. According to the EDS study, Nb and V precipitated out of the solution as grains and grain boundaries (Figure 5 c, e, g and Figure 6 c, e, g, k, m). The EDS line analysis also reveals that in Nb-V micro alloyed PM steels without Ni (S2 sample), the type and amount of elements varied along the line intersecting with the matrix and precipitates (see Figure 5 and Figure

6). It is accepted that precipitates detected in alloys by SEM and EDS tests have a significant effect on recrystallization and austenite grain development [56, 59].

During sintering after hot rolling or cooling for PM processing, microalloying elements such as Nb and V precipitate as niobium carbide (NbC), niobium nitride (NbN), and niobium carbonitride (NbCN). Significant increases in tensile and hardness strength occur in micro alloyed steels due to the grain refinement, precipitation hardening, and solid solution hardening mechanisms that are products of this process [56]. Although the average grain size of sample S1 was determined to be 36.8 µm, the average grain size of sample S2 was found to decrease to 30.5 µm due to precipitates such as VC(N) and NbC(N) formed during the sintering process. Furthermore, the development of austenite grains came to a halt due to the influence of these precipitates [18, 44, 60-62].

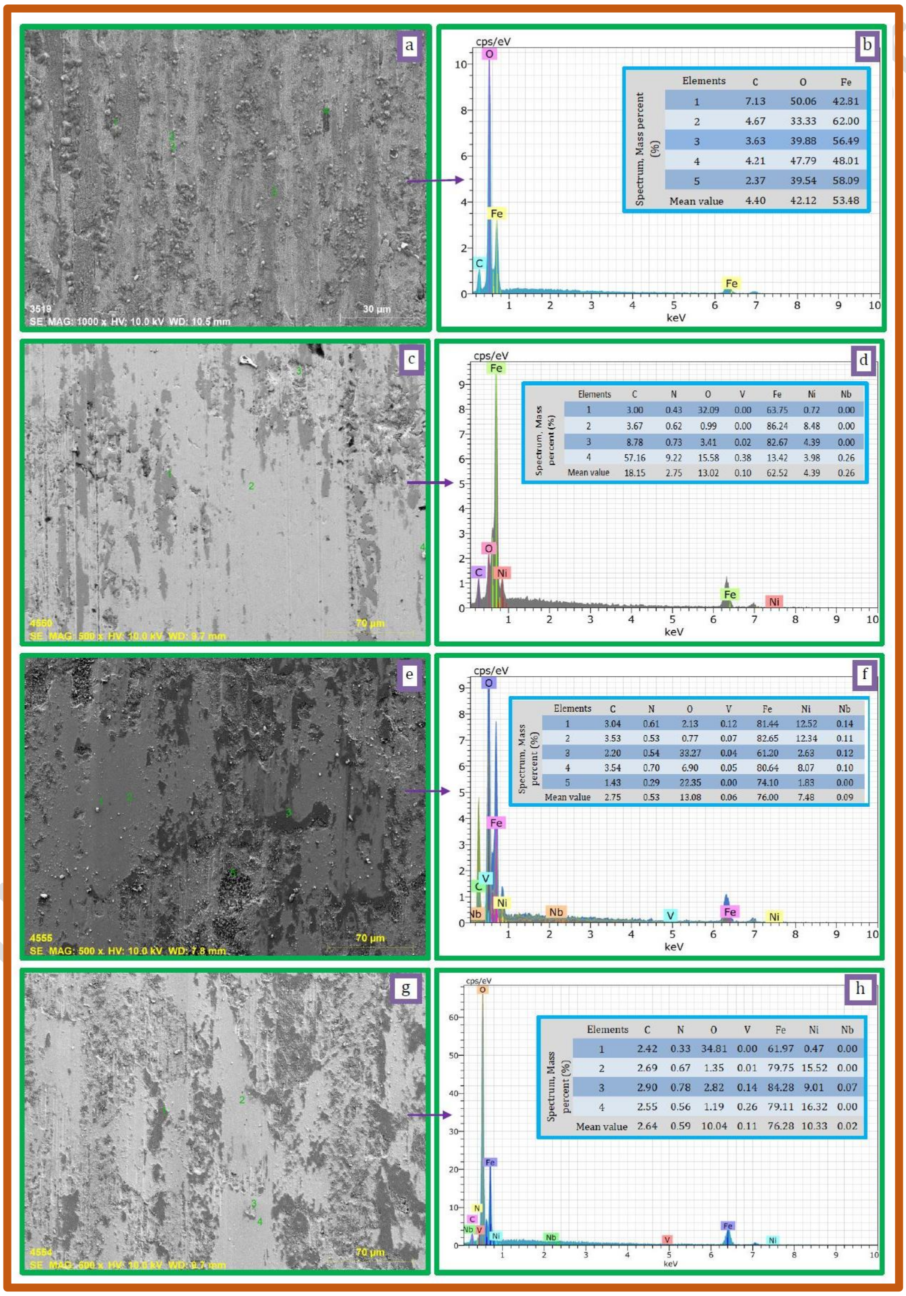

Figure 5. EDX analyses taken from dry wear surfaces at 30 N load; a) S1 surface points, b) S1 EDX peaks and elemental composition by weight, c) S3 surface points, d) S3 EDX peaks and elemental composition by weight, e) S5 surface points, f) S5 EDX peaks and elemental composition by weight, g) S5 surface points, h) S5 EDX peaks and elemental composition by weight

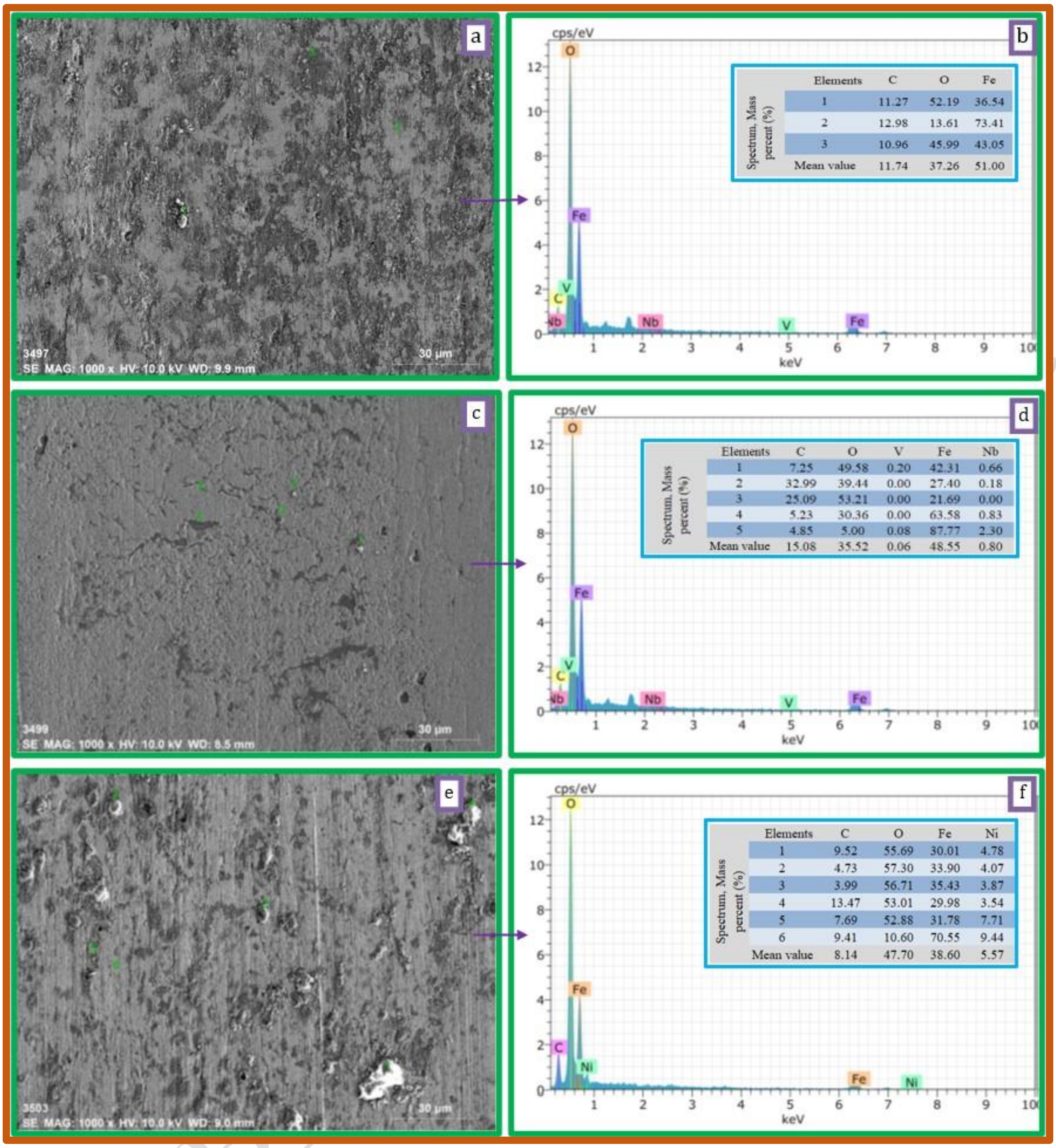
a
3497
SE MAG: 1000 x HV: 10.0 kV WD: 9.9 mm
30 µm
b
cps/eV
O
Fe
V
C
Nb
keV

Spectrum, Mass percent (%)

Elements	C	O	Fe
1	11.27	52.19	36.54
2	12.98	13.61	73.41
3	10.96	45.99	43.05
Mean value	11.74	37.26	51.00

c
3499
SE MAG: 1000 x HV: 10.0 kV WD: 8.5 mm
30 µm
d
cps/eV
O
Fe
V
C
Nb
keV

Spectrum, Mass percent (%)

Elements	C	O	V	Fe	Nb
1	7.25	49.58	0.20	42.31	0.66
2	32.99	39.44	0.00	27.40	0.18
3	25.09	53.21	0.00	21.69	0.00
4	5.23	30.36	0.00	63.58	0.83
5	4.85	5.00	0.08	87.77	2.30
Mean value	15.08	35.52	0.06	48.55	0.80

e
3503
SE MAG: 1000 x HV: 10.0 kV WD: 9.0 mm
30 µm
f
cps/eV
O
Fe
C
Ni
keV

Spectrum, Mass percent (%)

Elements	C	O	Fe	Ni
1	9.52	55.69	30.01	4.78
2	4.73	57.30	33.90	4.07
3	3.99	56.71	35.43	3.87
4	13.47	53.01	29.98	3.54
5	7.69	52.88	31.78	7.71
6	9.41	10.60	70.55	9.44
Mean value	8.14	47.70	38.60	5.57

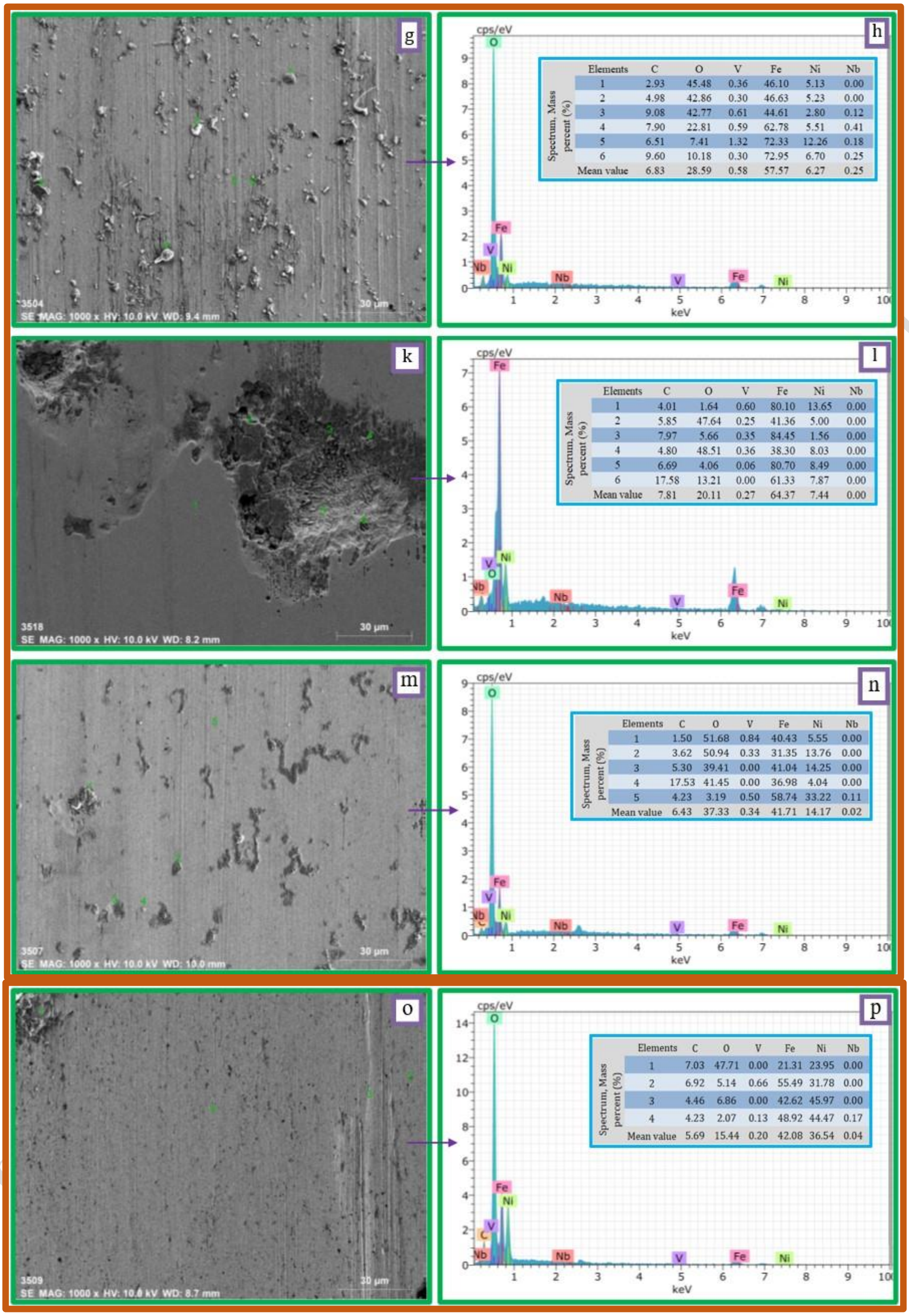

Figure 6. EDX analyses taken from dry wear surfaces at 30 N load; a) S1 surface points, b) S1 EDX peaks and elemental composition by weight, c) S2 surface points, d) S2 EDX peaks and elemental composition by weight, e) S3 surface points, f) S3 EDX peaks and elemental composition by weight, g) S4 surface points, h) S4 EDX peaks and elemental composition by weight, ı) S6 surface points, j) S6 EDX peaks and elemental composition by weight, k) S7 surface points, l) S7 EDX peaks and elemental composition by weight, m) S8 surface points, n) S8 EDX peaks and elemental composition by weight

The micrographs obtained at x500 magnification from the surfaces of the PM samples produced by pressing Fe-C and Fe-C-Nb-V, Fe-C-Nb-V -Ni powders at 700 MPa and then sintering at 1400 ºC in an Ar atmosphere after the wear test are shown in Figure 9 and Figure 10. When micrographs are examined, it is seen that the wear mechanism in steel produced with the PM technique occurs in a way that the abrasive ball generally creates lines parallel to the sliding direction. Additionally, it has been accepted that the addition of Ni to the alloy is effective in reducing wear depths. SEM wear images obtained from wear tracks reveal the presence of precipitates such as NbVCN, VC(N), NbV, VC, CV, FeV, Ni2V, and oxide structures such as FeO, FeOCNFeO, consistent with XRD analyses.

To further elucidate the phase constitution and microstructural characteristics of the steels containing different nickel additions, X-ray diffraction (XRD) analyses were performed, and the corresponding diffraction patterns are presented in Figure 7. The diffractograms exhibited a complex peak distribution arising from the coexistence of various phases associated with Fe, Ni, Nb, V, and C. Despite this complexity, the overall diffraction profiles were comparable among the samples investigated and were consistent with their respective alloying compositions. The incorporation of NbV promoted an increase in diffraction peak intensities, suggesting enhanced phase formation and crystallinity. In contrast, nickel addition resulted in a reduction in peak intensities, with a more pronounced decrease observed as the Ni content increased. As illustrated in Figure 7, this trend was evident across the entire diffraction range. Evaluation of the peak analysis data revealed that all specimens exhibited their maximum intensity at peak position 6. Phase characterization, consistent with the literature [55, 63, 64], revealed that in addition to carbide and nitride phases such as NbVCN, FeC, Fe_3C, and NbC, which are characteristic of the alloy systems studied, intermetallic compounds such as FeNi, $FeNi_3$, and Fe_3Ni_2 are also present in significant amounts.

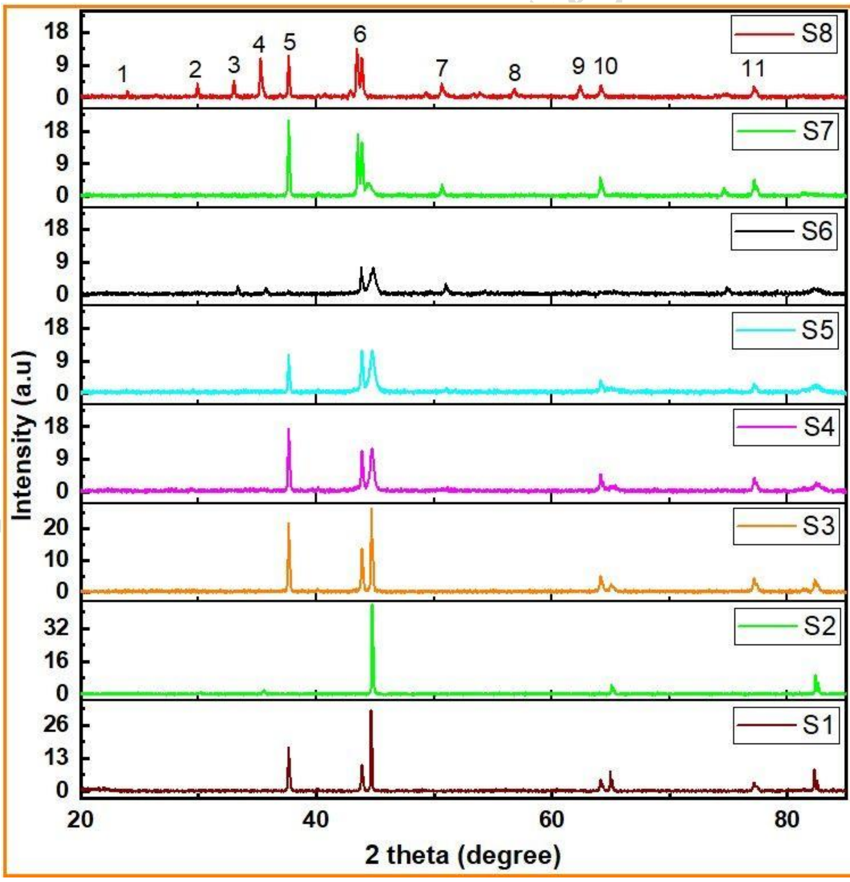

Formula	Pik Number
Fe	6, 7, 11
Fe, C	6, 7, 11
Fe_2C	5, 6, 8
Fe_3C	4, 5, 6, 7, 8, 9, 10, 11
Fe_5C_2	4, 5, 6, 7, 8, 11
Fe, Nb	4, 5, 6, 11
Fe_2Nb	2, 5, 6, 7, 8, 9, 11
Fe_2Nb_3	4, 5, 6
FeNi	6,7, 8, 11
Fe, Ni	2, 3, 4, 6,7, 8 11
$FeNi_3$	6,7, 11
Fe_3Ni_2	6, 7, 11
FeV	6, 10, 11
C	6, 11
C_{60}	1, 2, 3, 5, 6, 7
$C_{0.63}Fe_4$	6, 11
C_3Fe_7	6, 10, 11
C_5V_6	5, 6, 9, 11
VC	5, 6, 7, 9, 11
VCN	4, 6, 7, 10, 11
$VC_{0.75}$	5, 6, 10, 11
V_8C_7	5, 6, 9, 11
VFe	6, 10
V_3Fe_2	6, 10
NbC	4, 6, 10, 11
NbN	4, 6, 7, 10, 11
NbCN	4, 6, 7, 10, 11
Ni, Fe	6, 7, 11
Ni_2V	6, 7, 11
Ni_3V	6, 7, 11
Ni_8Nb	4, 5, 6, 7, 8, 11

Figure 7. XRD pattern of the samples

The presence of a liquid phase during sintering, such as at high temperatures of 1400 °C, is considered to significantly accelerate densification due to high Ni content and C content, facilitating particle rearrangement and diffusion-controlled mass transfer mechanisms. As a result, higher density levels and improved microstructural homogeneity are achieved compared to lower temperatures and shorter sintering times. However, the decrease in density at high Ni content in sample S8 is thought to be due to excessive Ni precipitation at the grain boundaries.

To examine the wear results in more detail, 3D topographic images were taken from the wear surfaces and are shown in Figure 8. The topography images obtained by the coloring made according to the difference of Ra values in the wear regions in the 3D topographic images helped to interpret the wear data more easily. When we look at the 3D topographic images shown in Figure 7, it is seen that the Ra values are lower because of the wear in the corrosive environment, which also supports the wear weight losses in Figure 3 and Figure 4. In the wear test carried out in a dry environment at a load of 30 N, the Ra value of sample S1 (Fe+C) was found to be 265 µm, while the Ra value of the same alloy in a corrosive environment was measured as 16 µm. S5 sample (Fe+C+0.15NbV+13Ni), which exhibited the lowest weight loss in wear tests, was 12 µm Ra value in the wear test performed under 30 N load, while Ra value was 6.1 µm in the wear test of the same alloy in a corrosive environment. In a corrosive environment, high wear resistance occurred because the corrosive fluid reduced deformation on the surface and internal structure of the material. This mechanism manifested itself in the reduced weight loss during the wear test. However, increased adhesion in the dry wear mechanism triggered irregular plastic deformation, which in turn led to an increase in Ra. Conversely, the corrosive wear fluid entering the wear zone removed heat from the wear environment, allowing for more controlled abrasive wear behavior. Consequently, material surface quality improved in the corrosive environment [65, 66].

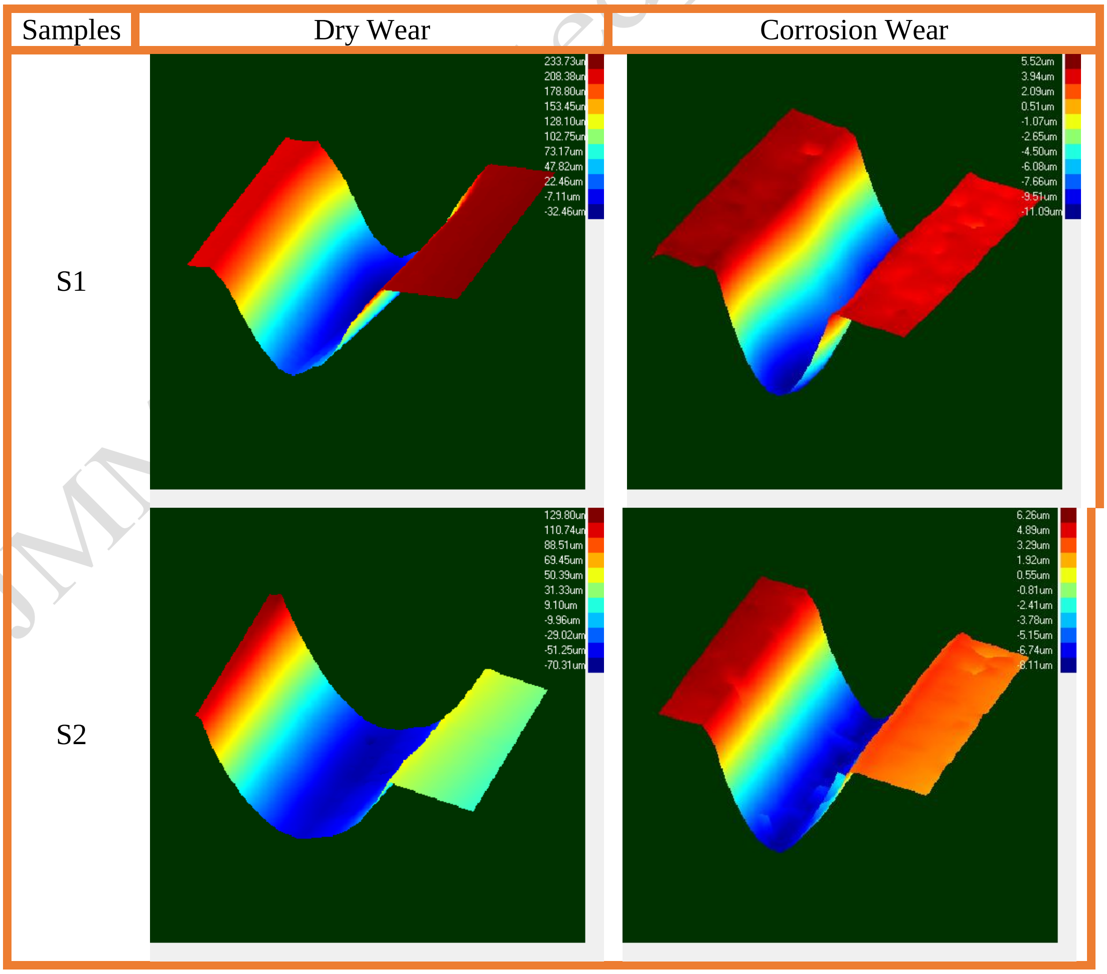

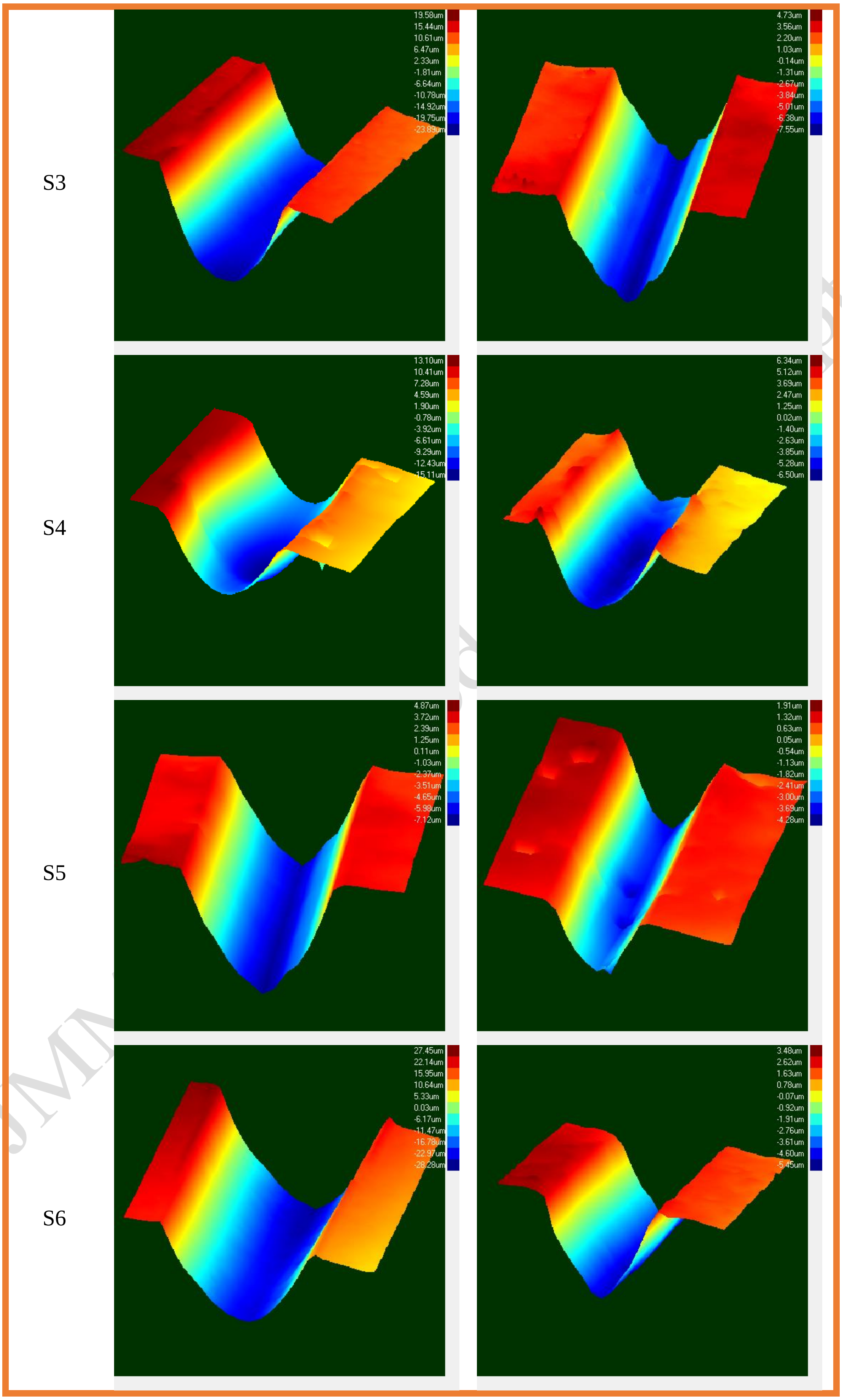
S3
S4
S5
S6
19.58um 15.44um 10.61um 6.47um 2.33um -1.81um -6.64um -10.78um -14.92um -19.75um -23.89um
4.73um 3.56um 2.20um 1.03um -0.14um -1.31um -2.67um -3.84um -5.01um -6.38um -7.55um
13.10um 10.41um 7.28um 4.59um 1.90um -0.78um -3.92um -6.61um -9.29um -12.43um -15.11um
6.34um 5.12um 3.69um 2.47um 1.25um 0.02um -1.40um -2.63um -3.85um -5.28um -6.50um
4.87um 3.72um 2.39um 1.25um 0.11um -1.03um -2.37um -3.51um -4.65um -5.98um -7.12um
1.91um 1.32um 0.63um 0.05um -0.54um -1.13um -1.82um -2.41um -3.00um -3.69um -4.28um
27.45um 22.14um 15.95um 10.64um 5.33um 0.03um -6.17um -11.47um -16.78um -22.97um -28.28um
3.48um 2.62um 1.63um 0.78um -0.07um -0.92um -1.91um -2.76um -3.61um -4.60um -5.45um

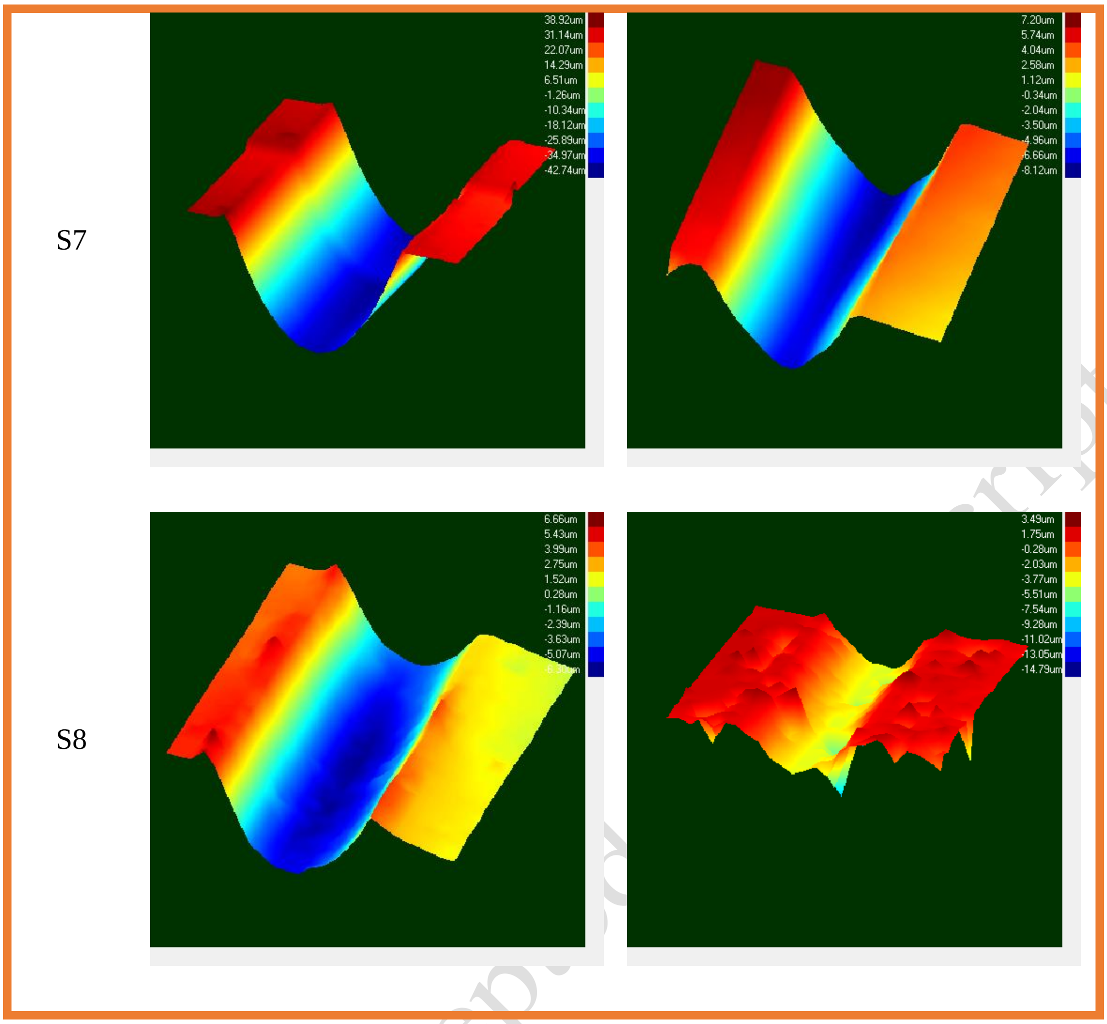

Figure 8. Surface topographies of samples worn in dry and corrosive environments at 30 N load

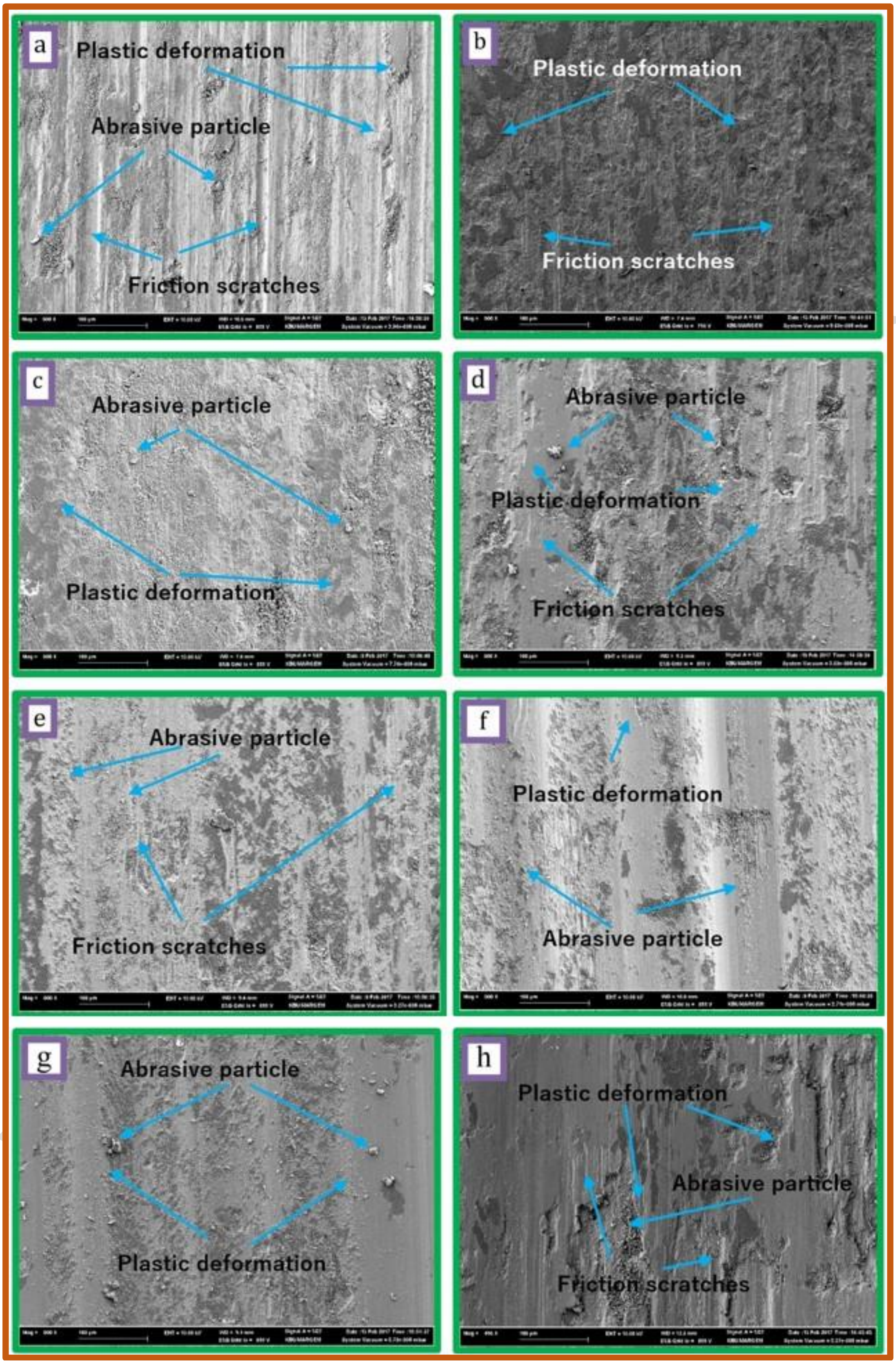

Figure 9. SEM images of dry wear surfaces at 30 N load 500x; a) S1, b) S2, s) S3, d) S4, e) S5, f) S6, g) S7, h) S8

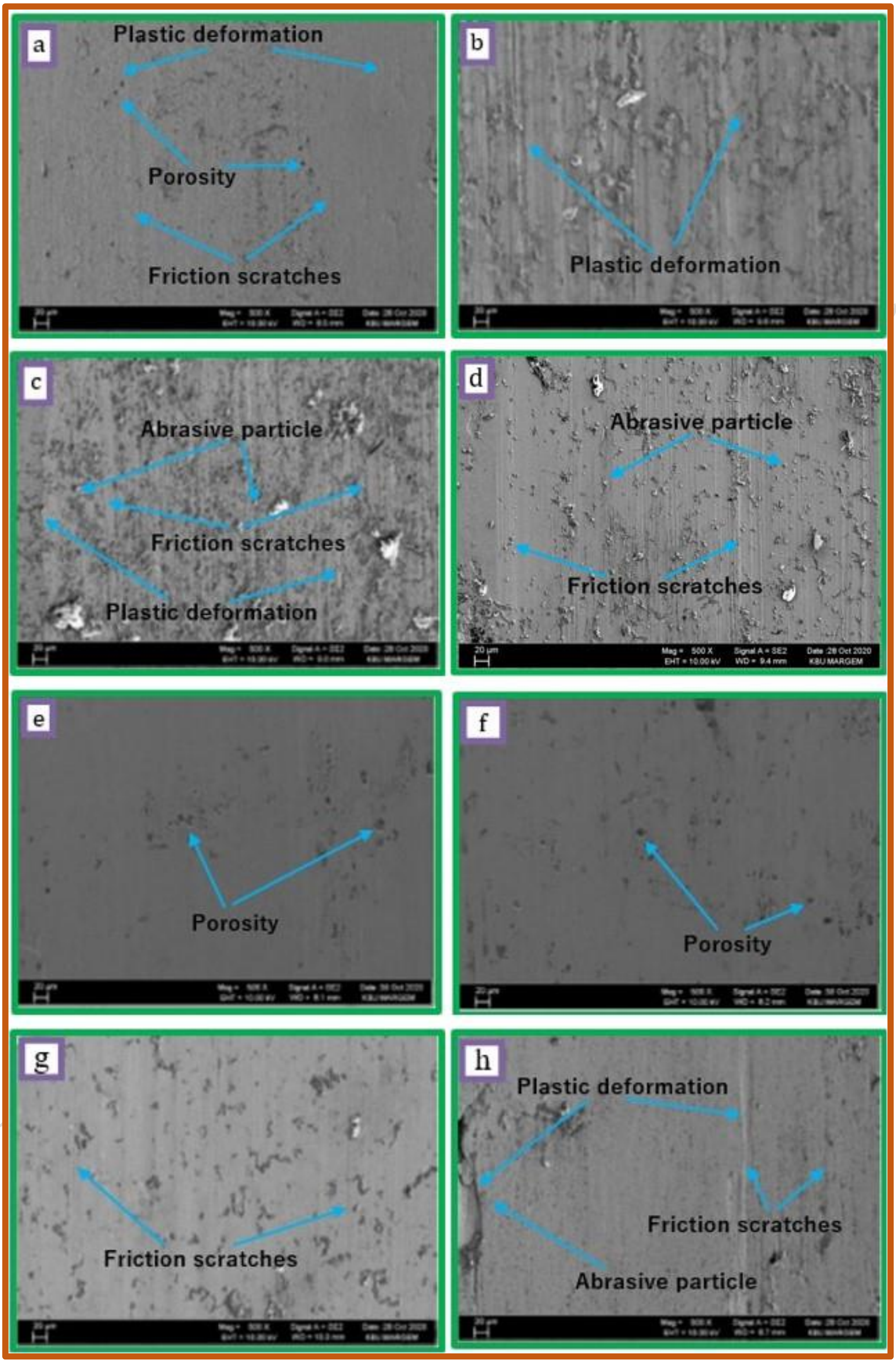

Figure 10. SEM images of corrosive wear surfaces at 30 N load 500x; a) S1, b) S2, s) S3, d) S4, e) S5, f) S6, g) S7, h) S8

All materials have wear channels according to the SEM pictures collected from the wear surfaces. Additionally, surface scratches developed shallower and thinner in the Nb-V doped sample, while they developed deeper and thicker in the unalloyed steel. This is consistent with the values for hardness. Erden et al. (2016) [18] reported that in the study on the friction-wear performance of the alloying element in micro-alloyed steel containing 0.1-0.15-0.2% Nb-Al powder by weight into the matrix, unalloyed steel showed the lowest wear resistance, while alloyed steel containing 2% Nb-Al gave better results in terms of wear resistance.

The observed deterioration in hardness and wear resistance when nickel content exceeds 13% can be attributed to several microstructural factors. First, the relatively low diffusion coefficient of nickel in iron restricts its homogenization during sintering and promotes localized Ni-rich regions and chemical decomposition within the matrix. This heterogeneity leads to an irregular phase distribution and reduces the effectiveness of precipitation strengthening mechanisms associated with Nb and V-containing carbides and carbonitrites [45, 46]. Furthermore, excessive nickel additions promote the stabilization of retained austenite and the formation of coarse austenitic regions with lower hardness than the bainitic and martensitic components that develop at moderate Ni levels [31, 46, 55]. SEM observations also revealed an increase in porosity with increasing nickel content. The higher porosity level can be associated with differences in particle size, morphology, and diffusion behavior between Ni and Fe powders; These differences hinder densification during sintering and reduce interparticle bonding efficiency [18, 42, 44, 45, 67]. These pores act as stress concentrates under shear contact and are preferred regions for crack formation and propagation, thus accelerating material loss during wear. Consequently, while moderate additions of Ni improve mechanical performance through microstructural refinement and phase transformation enhancement, excessive nickel content leads to microstructural inhomogeneity and increased porosity, ultimately reducing hardness and wear resistance.

Additionally, it was found that as the Nb-Al ratio improved, the alloys' hardness values also increased. When looking at the wear surfaces, it was determined that although all materials had the same wear mechanism, the wear lines became shallower and thinner as the amount of Nb-Al in the samples increased. As a result, the wear and hardness resistances were improved by including the Nb-V alloying element. Aggregation hardening, grain size reduction and precipitation hardening mechanisms caused by (N) in structures such as NbC(N), VC(N) and NbVC(N) are considered to be the cause of one or more of the strength-enhancing processes. The microstructures of the alloys containing 5% and 10% Ni are observed to consist of bainit grains and pearlite in which lamellar lengths of cementite and austenite grains shorter than those of pearlite (see Figure 9 and Figure 10). In alloys containing 13 weight percent Ni, austenite grains became more visible. Furthermore, rising Ni concentrations led to the appearance of inhomogeneous microstructures. Figure 4's mapping analysis for alloys 3 and 4 show that localized Ni segregation occurred when the Ni content increased from 5% to 10% due to the reduced Ni diffusion coefficient (see Figure 9 and Figure 10). Tracey and Upadyaya reported in their studies [44, 46], that elemental nickel diffuses more slowly than iron due to its lower diffusion coefficient compared to many elements such as carbon, copper, and molybdenum. This is explained by the fact that this situation causes inadequate dispersion during the sintering process. While the S6 sample with 15Ni ratio has an acicular martensitic structure with austenite grains, the S sample with 13Ni ratio has a pearlitic structure with austenite grains. In addition, while sample S8 with 30Ni content consists entirely of austenite grains, sample S7 with 20Ni content has a martensitic structure close to austenite grains.

Due to porosities, the samples' post-sintering densities are approximately 93%. Alloys created via powder metallurgy may include pores [67]. After sintering, the densities marginally increased. The results of related investigations provide evidence that the density rises during the sintering process [3, 18, 56, 61, 63]. During sintering, the pores between the powder particles are decreased, the contact points enlarge, and the neck formation takes place. In the neck's areas, grain boundaries are formed. As the grain boundaries widen, the material's structure becomes more uniform. In this investigation, it was found that the porosity in the microstructure pictures of the alloys increased as the amount of nickel increased. Compared to comparable alloys with lower Ni contents, alloy 8-30Ni has greater porosities. From here, it is reasonable to infer that low alloys are challenging to press and sinter due to the presence of various alloy constituents and the variations in their size and shape.

The creation of bainitic and martensitic structures is assumed to be triggered by an increase in the quantity of Ni added. Getting et al., in their study on [46] the effect of Ni addition on the mechanical properties of molybdenum PM steels, claimed that increasing the amount of Ni addition increased the hardness and tensile strength of the obtained PM steels. They also claimed that ferrite and pearlite make up the microstructure of molybdenum steel without nickel whereas the addition of nickel to 0-2% by weight results in tougher phases. The structure has bainitic and martensitic structure if nickel is supplied at a weight-based rate of 2% to 5%. Nickel diffuses into iron relatively slowly because, in comparison to many other elements including carbon, copper, and molybdenum, it has a low diffusion coefficient [44, 46].

Conclusion

The effects of nickel addition on the microstructure, hardness, and tribological behavior of Nb-V microalloyed powder metallurgy steels were systematically investigated under dry and corrosive sliding conditions. Based on the experimental findings, the following conclusions can be drawn:

1. The incorporation of Nb and V microalloying elements significantly refined the microstructure through the formation of fine carbide and carbonitride precipitates, including NbC, VC, and Nb(V)(C,N). These precipitates effectively restricted grain growth during sintering and contributed to precipitation strengthening, resulting in improved hardness and wear resistance compared with the unalloyed steel.
2. Nickel addition strongly influenced the phase constitution and microstructural evolution of the PM steels. Increasing Ni content promoted the formation of bainitic, martensitic, and austenitic regions, while also enhancing densification and mechanical performance up to an optimum concentration.
3. The alloy containing 13 wt.% Ni (S5) exhibited the best overall performance, achieving the highest hardness value (244 HV0.5) and the lowest wear losses under both dry and corrosive sliding conditions. Under a dry sliding load of 30 N, the wear loss decreased from 35.866 mg for the unalloyed steel to 7.367 mg for the S5 alloy, corresponding to an improvement of approximately 79%.
4. XRD analyses confirmed the presence of strengthening carbide phases such as Fe_3C and NbC together with Fe-Ni intermetallic compounds including FeNi, $FeNi_3$, and Fe_3Ni_2. The combined strengthening effects of these phases contributed significantly to the enhanced hardness and tribological performance of the microalloyed steels.
5. Wear resistance was consistently higher in the corrosive sliding environment than in dry sliding conditions. The NaCl solution acted as a cooling and lubricating medium, reducing frictional heating, limiting severe plastic deformation, and consequently decreasing material loss and surface roughness.
6. Excessive nickel additions (>13 wt.%) resulted in a deterioration of hardness and wear performance. This behavior was associated with microstructural heterogeneity caused by nickel segregation, stabilization of retained austenite, and increased porosity arising from the limited diffusion rate of nickel during sintering. These factors reduced matrix uniformity and promoted crack initiation during sliding wear.

7. SEM observations revealed that abrasive wear was the dominant wear mechanism for all alloys. However, the depth and severity of wear grooves decreased considerably with Nb–V microalloying and moderate nickel additions, confirming the beneficial role of microstructural refinement and precipitation hardening in enhancing wear resistance.

Overall, the results demonstrate that the synergistic combination of Nb–V microalloying and controlled nickel addition provides an effective approach for optimizing the microstructure and tribological performance of powder metallurgy steels. Among the investigated compositions, the alloy containing 13 wt.% Ni offered the most favorable balance between hardness, density, and wear resistance, making it a promising candidate for engineering applications requiring high durability under both dry and corrosive service environments.

Contributions of the authors: M.A.E. and M.A. designed the experiments; M.A.E., H.C., and M.A.M.A. carried out the experiments; M.A.E., M.A.M.A., B.G. and H.C., M.A.E. analyzed the data and wrote the paper; M.A.E., M.A.M.A., B.G. and H.C., and M.A.E. directed

Support: There was no outside funding for this study.

Recognitions: Mohamed Ahmed Mohamed Ahssi completed this research as part of his doctoral dissertation at Karabuk University in Karabuk, Turkey.

Conflicts of Interest: The authors say they have none.

References

[1]. T. Williams, R. Nanstad, Low-alloy steels, in Structural Alloys for Nuclear Energy Applications, Elsevier, 2019, pp. 411-483. https://doi.org/10.1016/B978-0-12-397046-6.00010-1

[2]. Z. Cheng, M. Gao, J. Liu, S. Wang, G. Wu, J. Gao, H. Wu, X. Mao, Multi-scale microstructural tailoring and associated properties of press-hardened steels: a review, *Materials*, **16**(10), (2023) 3799. https://doi.org/10.3390/ma16103799

[3]. M.A. Erden, The effect of the sintering temperature and addition of niobium and vanadium on the microstructure and mechanical properties of microalloyed PM steels, *Metals*, (2017), **7**(9), 329. https://doi.org/10.3390/met7090329

[4]. C.E.G. Cortopassi, M.L.A. Cunha, V.S. Barbosa, M.M. Leivas, J.H. Alano, K.E. Bianc hi, H.L. Costa, Effect of Microalloying and Thermomechanical Treatment on the Low-Temperature Fracture Toughness of a High-Strength Weathering Steel, *Journal of Materials Research and Technology*, (2025) **36** 2033-204. https://doi.org/10.1016/j.jmrt.2025.03.160

[5]. B.F. Kinaci, M.A. Erden, H.Çuğ, C.Özarpa, B. Çiçek, *Effect of Sinter Temperature and Thermochemical Coating on Mechanical Properties of Ti 6 Al 4 V Produced by Powder Metallurgy, Journal of Molecular & Engineering Materials*, **13**(3) (2025) 18539420. https://doi.org/10.1142/S2251237325500054

[6]. C.T.J. Panicker, V. Senthilkumar, Enhancing low-alloy steel produced by rotational arc-WAAM (RA-WAAM): impact of nickel–chromium powders on mechanical, microstructural, and corrosion properties, *Progress in Additive Manufacturing*, (2025) 1-12. https://doi.org/10.1007/s40964-025-01001-y

[7]. W.J. Joost, Reducing vehicle weight and improving US energy efficiency using integrated computational materials engineering. *Jom*, **64** (2012) 1032-1038. https://doi.org/10.1007/s11837-012-0424-z
[8]. E. De Moor, Advanced high-strength sheet steels for automotive applications. *High-Performance Ferrous Alloys*, (2021) 113-151. https://doi.org/10.1007/978-3-030-53825-5_4
[9]. M.J. Santofimia, L. Zhao, R. Petrov, C. Kwakernaak, W.G. Sloof, J. Sietsma, Microstructural development during the quenching and partitioning process in a newly designed low-carbon steel, *Acta Materialia*, 2011, **59**(15), p. 6059-6068. https://doi.org/10.1016/j.actamat.2011.06.014
[10]. S. Gündüz, H. Karabulut, M.A. Erden, M. Türkmen, Microstructural effects on fatigue behaviour of a forged medium carbon microalloyed steel, *Materials Testing*, **55**(11-12) (2013) 865-870. https://doi.org/10.3139/120.110511
[11]. J.C. Villalobos, A. Del-Pozo, B. Campillo, J. Mayen, S. Serna, Microalloyed steels through history until 2018: Review of chemical composition, processing and hydrogen service, *Metals*, **8**(5) (2018) 351. https://doi.org/10.3390/met8050351
[12]. G. Xu, X. Gan, G. Ma, F. Luo, H. ZouXu, The development of Ti-alloyed high strength microalloy steel, *Materials & Design*, **31**(6) (2010) 2891-2896. https://doi.org/10.1016/j.matdes.2009.12.032
[13]. V.L. Nuam, H. Zhang, Y.C. Wang, Z.P. Xiong, Role of retained austenite in advanced high-strength steel: ductility and toughness, *Journal of Iron and Steel Research International*, **31**(9) (2024) 2079-2089. https://doi.org/10.1016/j.matchar.2025.115282
[14]. C. Meng, Y. Wang, Y. Wei, B. Shi, T. Cui, Y. Wang, Strengthening mechanisms for Ti- and Nb-Ti-micro-alloyed high-strength steels, *Journal of Iron and Steel Research International*, **23**(4) (2016) 350-356. https://doi.org/10.1016/S1006-706X(16)30056-5
[15]. B. Verlinden, J. Driver, I. Samajdar, R.D. Doherty, Thermo-mechanical processing of metallic materials. *Elsevier*, **11 (**2007) 1-491.
[16]. Y. Lai, H. Luo, C. Xu, L. Yang, J. Zhang, J. Cao, X. Zhou, X. Xiong, X. Ye, C. Wang, Effect of Final Rolling Temperature on Microstructure, Mechanical Properties, and Strengthening Mechanism of High-Strength Ti–Zr Composite Microalloyed Steels, *Metal Science and Heat Treatment*, **66**(9) (2025) 635-645. https://doi.org/10.1007/s11041-025-01097-7
[17]. M. Jahazi, B. Egbali, The influence of hot rolling parameters on the microstructure and mechanical properties of an ultra-high strength steel, *Journal of materials processing technology*, **103**(2) (2000) 276-279. https://doi.org/10.1016/S0924-0136(00)00474-X
[18]. M.A. Erden, S. Gündüz, H. Karabulut, M. Türkmen, Effect of vanadium addition on the microstructure and mechanical properties of low carbon micro-alloyed powder metallurgy steels, *Materials Testing*, **58**(5) (2016) 433-437. https://doi.org/10.3139/120.110875
[19]. L. Chang, Y.S. Hwang, Effect of vanadium content and annealing temperature on recrystallisation, grain growth, and magnetic propertiesin 0-3% Si electrical steels, *Materials science and technology*, **14**(7) (1998) 608-618. https://doi.org/10.1179/mst.1998.14.7.608
[20]. M.E.E. Erhaime, H. Cug, M.A. Erden, Y. Akgul, A. Incesu, B. Cicek, Synergetic Effect of Nb–V on Mechanical, Tribological and Corrosion Properties of AISI 603 Steel

Produced via Powder Metallurgy, *Journal of Molecular & Engineering Materials*, **13**(2) (2025) 2550002.
https://doi.org/10.1142/S2251237325500029

[21]. C. Schade, T. Murphy, A. Lawley, R. Doherty, Microstructure and mechanical properties of microalloyed PM steels, *International Journal of Powder Metallurgy*, **48**(3) (2012) 51-59.

[22]. Y. Li, Y. Lu, W. Li, M. Khedr, H. Liu, X. Jin, Hierarchical microstructure design of a bimodal grained twinning-induced plasticity steel with excellent cryogenic mechanical properties, *Acta Materialia*, **158 (**2018) 79-94.
https://doi.org/10.1016/j.actamat.2018.06.019

[23]. B.C. De Cooman, Y. Estrin, S.K. Kim, Twinning-induced plasticity (TWIP) steels, *Acta Materialia*, **142 (**2018) 283-362.
https://doi.org/10.1016/j.actamat.2017.06.046

[24]. Y. Ju, A. Goodall, M. Strangwood, C. Davis, Characterisation of precipitation and carbide coarsening in low carbon low alloy Q&T steels during the early stages of tempering, *Materials Science and Engineering: A*, **738 (**2018) 174-189.
https://doi.org/10.1016/j.msea.2018.09.044

[25]. F. Liu, K. Chen, C. Kang, Z. Jiang, S. DingLiu, Effects of V–Nb microalloying on the microstructure and properties of spring steel under different quenching-tempering times, *Journal of Materials Research and Technology*, **19 (**2022) 779-793.
https://doi.org/10.1016/j.jmrt.2022.05.043

[26]. Z. Yan, K. Liu, J. Eckert, Effect of tempering and deep cryogenic treatment on microstructure and mechanical properties of Cr–Mo–V–Ni steel, *Materials Science and Engineering: A*, **787 (**2020) 139520.
https://doi.org/10.1016/j.msea.2020.139520

[27]. C.P. Scott, F. Fazeli, B. Shalchi Amirkhiz, I. Pushkareva, S.Y.P. Allain, Structure-properties relationship of ultra-fine grained V-microalloyed dual phase steels, *Materials Science and Engineering: A*, **703 (**2017) 293-303.
https://doi.org/10.1016/j.msea.2017.07.051

[28]. Z. Wang, W. Hui, Z. Chen, Y. Zhang, X. Zhao, Effect of vanadium on microstructure and mechanical properties of bainitic forging steel, *Materials Science and Engineering: A*, **771** (2020) 138653.
https://doi.org/10.1016/j.msea.2019.138653

[29]. Y. Zhang, Y. Ma, Research Progress on Titanium–Niobium Micro-Alloyed High-Strength Steel, *Materials*, **18**(2) (2025) 325.
https://doi.org/10.3390/ma18020325

[30]. H. Karabulut, M. Türkmen, M.A. Erden. S. Gündüz, Effect of different current values on microstructure and mechanical properties of microalloyed steels joined by the submerged arc welding method, *Metals*, **6**(11) (2016) 281.
https://doi.org/10.3390/met6110281

[31]. T. Gladman, Physical metallurgy of microalloyed steels, *Maney Publishing*, 2002, pp. 383.

[32]. S. Gündüz, M.A. Erden, H. Karabulut, M. Türkmen, Effect of The Addition of Nioibium and Aluminium on the Microstructures And Mechanical Properties of Microalloyed PM Steels. *Materiali in Tehnologije*, **50**(5) (2016) 641-648.
https://doi.org/10.17222/mit.2015.248

[33]. C.P. Scott, B.S. Amirkhiz, I. Pushkareva, F. Fazeli, S.Y.P. Allain, H. Azizi, New insights into martensite strength and the damage behaviour of dual phase steels, *Acta Materialia*, **159 (**2018) 112-122.
https://doi.org/10.1016/j.actamat.2018.08.010

[34]. J. Samei, L. Zhou, J. Kang, D.S. Wilkinson, Microstructural analysis of ductility and fracture in fine-grained and ultrafine-grained vanadium-added DP1300 steels, *International Journal of Plasticity*, **117** (2019) 58-70. https://doi.org/10.1016/j.ijplas.2017.12.009
[35]. Y. Li, J. Li, D. Zhang, Q. Pang, Strain-Induced Precipitation Behavior of V Microalloyed High Manganese Steel, *Materialia*, **40** (2025) 102392. https://doi.org/10.1016/j.mtla.2025.102392
[36]. C.R. Hutchinson, H.S. Zurob, C.W. Sinclair, Y.J.M. Brecheti, The comparative effectiveness of Nb solute and NbC precipitates at impeding grain-boundary motion in Nb steels, *Scripta Materialia*, **59**(6) (2008) 635-637. https://doi.org/10.1016/j.scriptamat.2008.05.036
[37]. Y. Gu, G. Qiao, D. Wu, B. Liao, F. Xiao, Precipitation kinetics of Nb carbonitride in austenite and acicular ferrite and its effect on hardness of high-Nb steel, *Materials Chemistry and Physics*, **183** (2016) 506-515. https://doi.org/10.1016/j.matchemphys.2016.09.008
[38]. C.P. Massey, D.T. Hoelzer, R.L. Seibert, P.D. Edmondson, A. Kini, B. Gault, K.A. Terrani, S.J. Zinkle, Microstructural evaluation of a Fe-12Cr nanostructured ferritic alloy designed for impurity sequestration, *Journal of Nuclear Materials*, **522** (2019) 111-122. https://doi.org/10.1016/j.jnucmat.2019.05.019
[39]. L. Sun, X. Liu, X. Xu, S. Lei, H. Li, Q. Zhai, Review on niobium application in microalloyed steel, *Journal of Iron and Steel Research International*, **29**(10) (2022) 1513-1525. https://doi.org/10.1007/s42243-022-00789-1
[40]. R.B. Calhoun, D.C. Dunand, Dislocations in metal matrix composites: metal matrix composites, in Comprehensive Composite Materials: Metal Matrix Composites, Elsevier, 2000, pp. 27-59.
[41]. .R. Ke, C. Hu, M. Zhong, X. Wan, K. WuKe, Grain refinement strengthening mechanism of an austenitic stainless steel: critically analyze the impacts of grain interior and grain boundary, *Journal of Materials Research and Technology*, **17** (2022) 2999-3012. https://doi.org/10.1016/j.jmrt.2022.02.056
[42]. M. Meignanamoorthy, M. Ravichandran, Synthesis of metal matrix composites via powder metallurgy route. *Mechanics and Mechanical Engineering*, **22**(1) (2018) 65-75.
[43]. D. Özdemirler, S. Gündüz, M.A. Erden, Influence of NbC addition on the sintering behaviour of medium carbon PM steels, *Metals*, **7**(4) (2017) 121. https://doi.org/10.3390/met7040121
[44]. G.S. Upadhyaya, Sintered metallic and ceramic materials: preparation, proerties and applications. 2000, West Sussex, UK: JohnWiley & Sons Ltd, 2000.
[45]. Q. Ma, S. Jia, Q. Liu, C. Shang, Effects of Cr and Ni addition on critical crack tip opening displacement (CTOD) and supercritical CO2 corrosion resistance of high-strength low-alloy steel (HSLAs), *Materials Science and Engineering: A*, **908** (2024) 146772. https://doi.org/10.1016/j.msea.2024.146772
[46]. V. Tracey, Nickel sintered steels-Developments, status and prospects, *Metal Powder Report*, **47**(11) (1992) 49.
[47]. W.Yu, Y. Feng, T. Guo, W. Wu, J. Zhang, Insight into the Ni microalloying effects on the corrosion characteristics and mechanism of Fe-21Mn-10Al-1.25 C lightweight steels in chloride-containing solution, *Construction and Building Materials*, **456** (2024) 139313.

https://doi.org/10.1016/j.conbuildmat.2024.139313
[48]. H. Zhang, W.-X. Wang, F. Chang, C.-L. Li, S.-L. Shu, Z.-F. Wang, X. Han, Q. Zou, F. Qiu, Q. Jiang, Microstructure manipulation and strengthening mechanisms of 40Cr steel via trace TiC nanoparticles. *Materials Science and Engineering: A*, **822** (2021) 141693. https://doi.org/10.1016/j.msea.2021.141693
[49]. Y. Zhang, Y. Ma, Research progress on titanium–niobium micro-alloyed high-strength steel. *Materials*, **18**(2) (2025) 325. https://doi.org/10.3390/ma18020325
[50]. L. Bao, L. Xiong, Q. Zhang, W. Liang, X. Li, G. Xu, S. Sang, Q. Yuan,Tailoring Microstructure and Strength Contribution in a Mo–Nb–Ti Tempering Steel via Controlled Coiling and Tempering Temperatures. *steel research international*. (2026) 1-16. https://doi.org/10.1002/srin.202501284
[51]. Z. Ni, J. Zhao, X. Wang, C. Shang, W. Zhou, New insights from crystallography into the effect of Ni content on ductile-brittle transition temperature of 1000 MPa grade high-strength low-alloy steel. *Journal of Materials Research and Technology*, **33** (2024) 589-599. https://doi.org/10.1016/j.jmrt.2024.09.072
[52]. ASTM, Test Method for Density, Oil Content, and Interconnected Porosity of Sintered Metal Structural Parts and Oil-Impregnated Bearings-B328-96. ASTM International: West Conshohocken, PA, USA, 2017, pp. 1-4.
[53]. H. Fischmeister, Applications of quantitative microscopy in materials engineering. *Journal of Microscopy*, **95**(1) (1972) 119-143. https://doi.org/10.1111/j.1365-2818.1972.tb03715.x
[54]. ASTM, Standard test methods for determining average grain size-E112-96. 2025, ASTM International: West Conshohocken, PA, USA, 2025, pp. 1-5.
[55]. M.A.M. Ahssi, M.A. Erden, M. Acarer, H. Çuğ, The effect of nickel on the microstructure, mechanical properties and corrosion properties of niobium–vanadium microalloyed powder metallurgy steels. *Materials*, **13**(18) (2020) 4021. https://doi.org/10.3390/ma13184021
[56]. M.A. Erden, S. Gündüz, M. Türkmen, H. Karabulut, Microstructural characterization and mechanical properties of microalloyed powder metallurgy steels. *Materials Science and Engineering: A*, **616,** (2014) 201-206. https://doi.org/10.1016/j.msea.2014.08.026
[57]. B. Białobrzeska, R. Jasiński, R. Dziurka, P. Bała, Effect of chromium and titanium on the microstructure and mechanical properties of cast steel. *Journal of Mining and Metallurgy, Section B: Metallurgy*, **60**(2), (2024) 235-257. https://doi.org/https://doi.org/10.2298/JMMB240424023B
[58]. S.K. Mishra, S. Das, S. Ranganathan, Precipitation in high strength low alloy (HSLA) steel: a TEM study, *Materials Science and Engineering: A*, **323**(1-2) (2002) 285-292. https://doi.org/10.1016/S0921-5093(01)01382-X
[59]. M. Türkmen, M.A. Erden, H. Karabulut, S. Gündüz, The effects of heat treatment on the microstructure and mechanical properties of Nb–V microalloyed powder metallurgy steels, *Acta Phys. Pol. A*, **135** (2019) 834-836. https://doi.org/10.12693/APhysPolA.135.834
[60]. R. Sepúlveda, F. Arenas, TiC–VC–Co: a study on its sintering and microstructure, *International Journal of Refractory Metals and Hard Materials*, **19**(4-6) (2001) 389-396. https://doi.org/10.1016/S0263-4368(01)00013-0

[61]. X.d. Huo, X.-p. Mao, S.-x. Lü, Effect of Annealing Temperature on Recrystalization Behavior of Cold Rolled Ti-Microaloyed Steel, *Journal of Iron and Steel Research International*, **20**(9) (2013) 105-110. https://doi.org/10.1016/S1006-706X(13)60164-8

[62]. M.A. Erden, The effect of sintering time on tensile strength of NB-V microalloyed powder metallurgy steels, *Technological Applied Sciences*, **15**(1) (2020) 15-22. https://doi.org/10.12739/NWSA.2020.15.1.2A0180

[63]. H. Zhao, G. Yu, X. Guo, F. Luo, F. Zhu, Y. Lei, Preparation of Ni-Based Composite Coatings on the Inner Surfaces of Tubes via Cylindrical Electro-Spark Powder Deposition. *Coatings*, **15**(12) (2025) 1426. https://doi.org/10.3390/coatings15121426

[64]. S. Khan, Khadija, M. Junaid, T. Shehbaz, F.N. Khan, Evaluations of nanomechanical and indentation creep of diffusion-bonded aluminum and austenitic stainless steel joint interface. *Proceedings of the Institution of Mechanical Engineers, Part L: Journal of Materials: Design and Applications*, **239**(7), (2025) 1353-1365. https://doi.org/https://doi.org/10.1177/14644207241290447

[65]. M.H. Cetin, S. Korkmaz, Investigation of the concentration rate and aggregation behaviour of nano-silver added colloidal suspensions on wear behaviour of metallic materials by using ANOVA method, *Tribology International*, **147** (2020) 106273. https://doi.org/10.1016/j.triboint.2020.106273

[66]. H.A. Raghs, B. Kondul, M.H. Cetin, Investigation of wear behavior of boronized H13 steel under environment of nano-silver-added lubricants coated with different ligands, *Surface Topography: Metrology and Properties*, 2020, **8**(1), p. 015007. https://doi.org/10.1088/2051-672X/ab6ece

[67]. N. Alharthi, E.S.M. Sherif, H.S. Abdo, S.Z.E. Abedin, Effect of Nickel Content on the Corrosion Resistance of Iron-Nickel Alloys in Concentrated Hydrochloric Acid Pickling Solutions, Advances in Materials Science and Engineering, **2017**(1) (2017) 1893672. https://doi.org/10.1155/2017/1893672

Figure List

Figure 1.

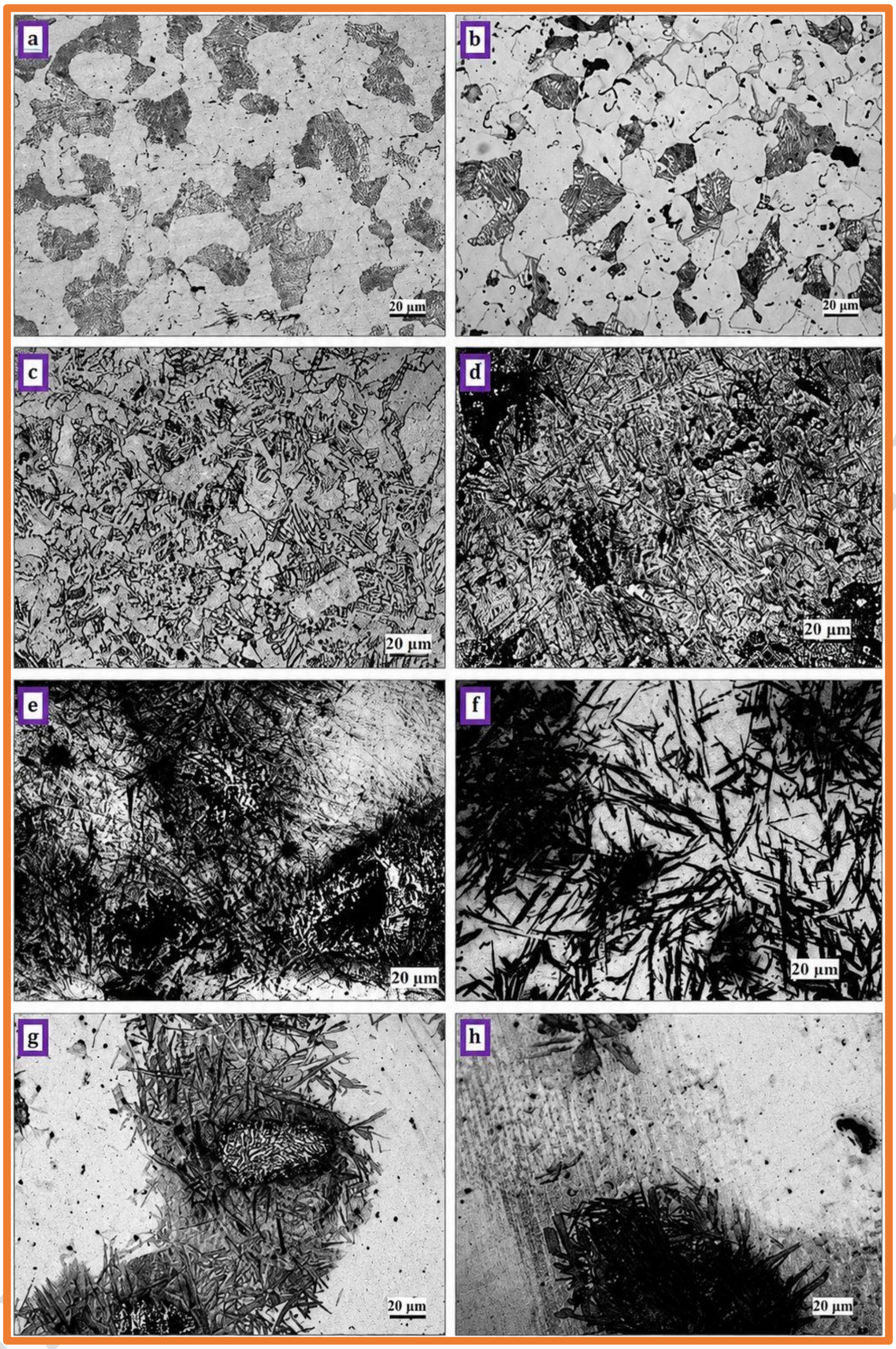

Figure 2.

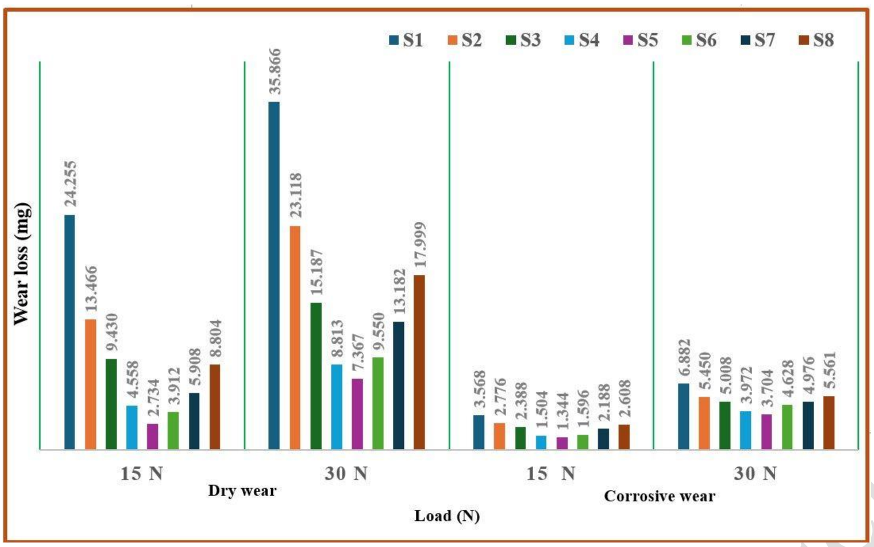

Figure 3.

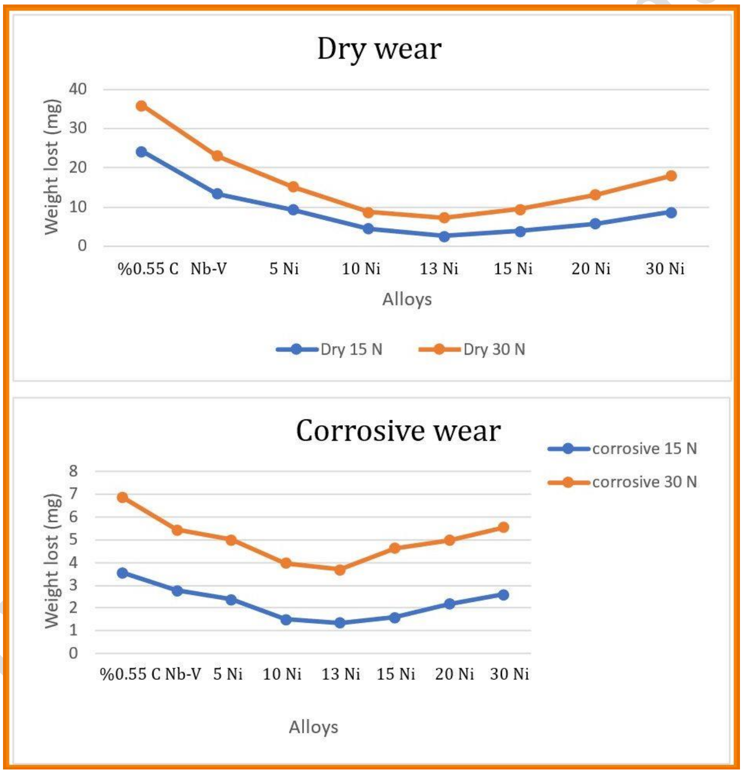

Figure 4.

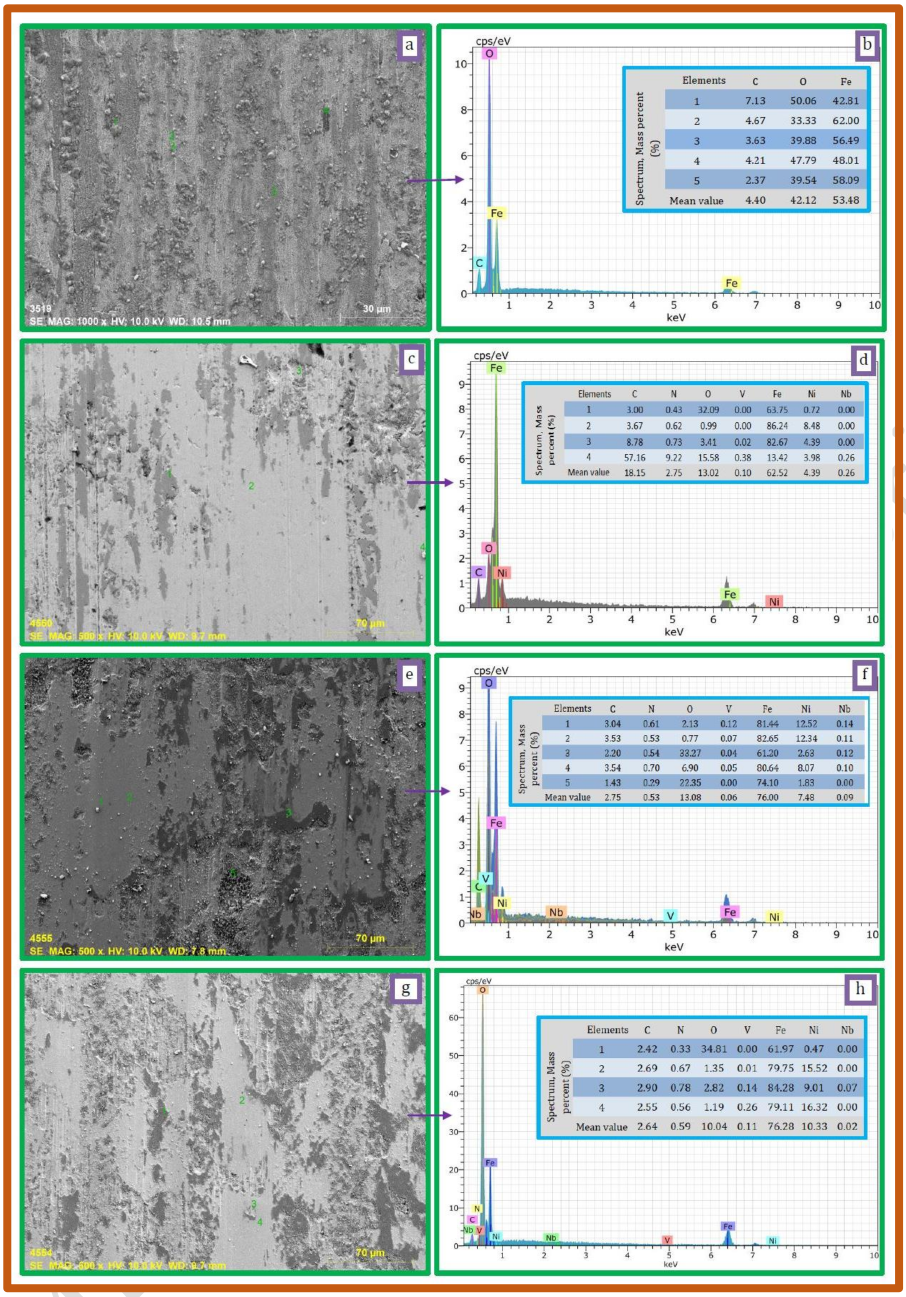

a
b
c
d
e
f
g
h
cps/eV
keV
SE MAG: 1000 x HV: 10.0 kV WD: 10.5 mm
30 µm
SE MAG: 500 x HV: 10.0 kV WD: 7.8 mm
70 µm

Spectrum, Mass percent (%)

Elements	C	O	Fe
1	7.13	50.06	42.81
2	4.67	33.33	62.00
3	3.63	39.88	56.49
4	4.21	47.79	48.01
5	2.37	39.54	58.09
Mean value	4.40	42.12	53.48

Spectrum, Mass percent (%)

Elements	C	N	O	V	Fe	Ni	Nb
1	3.00	0.43	32.09	0.00	63.75	0.72	0.00
2	3.67	0.62	0.99	0.00	86.24	8.48	0.00
3	8.78	0.73	3.41	0.02	82.67	4.39	0.00
4	57.16	9.22	15.58	0.38	13.42	3.98	0.26
Mean value	18.15	2.75	13.02	0.10	62.52	4.39	0.26

Spectrum, Mass percent (%)

Elements	C	N	O	V	Fe	Ni	Nb
1	3.04	0.61	2.13	0.12	81.44	12.52	0.14
2	3.53	0.53	0.77	0.07	82.65	12.34	0.11
3	2.20	0.54	33.27	0.04	61.20	2.63	0.12
4	3.54	0.70	6.90	0.05	80.64	8.07	0.10
5	1.43	0.29	22.35	0.00	74.10	1.83	0.00
Mean value	2.75	0.53	13.08	0.06	76.00	7.48	0.09

Spectrum, Mass percent (%)

Elements	C	N	O	V	Fe	Ni	Nb
1	2.42	0.33	34.81	0.00	61.97	0.47	0.00
2	2.69	0.67	1.35	0.01	79.75	15.52	0.00
3	2.90	0.78	2.82	0.14	84.28	9.01	0.07
4	2.55	0.56	1.19	0.26	79.11	16.32	0.00
Mean value	2.64	0.59	10.04	0.11	76.28	10.33	0.02

Figure 5.

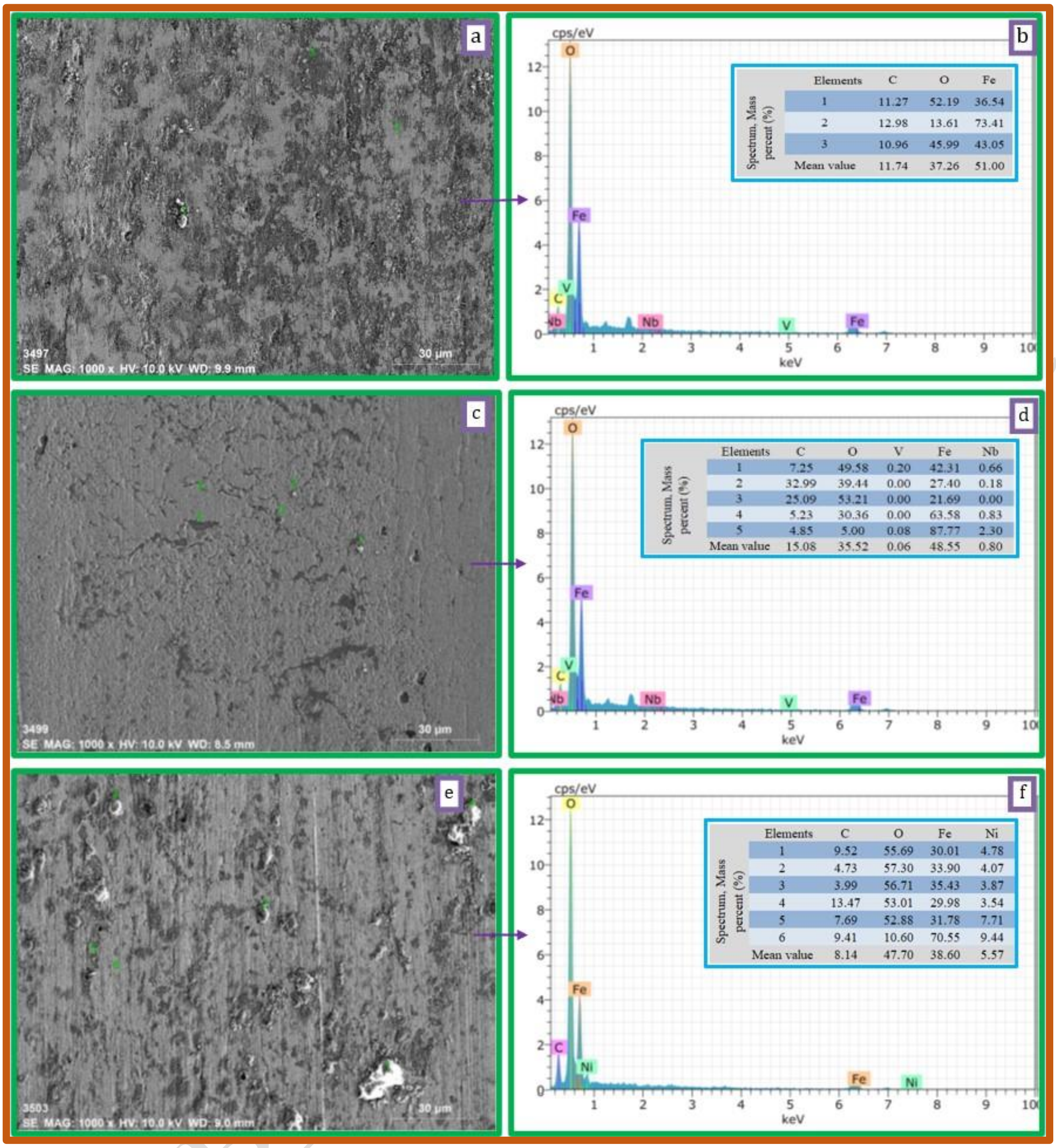

Spectrum, Mass percent (%) Elements	C	O	Fe
1	11.27	52.19	36.54
2	12.98	13.61	73.41
3	10.96	45.99	43.05
Mean value	11.74	37.26	51.00

Spectrum, Mass percent (%) Elements	C	O	V	Fe	Nb
1	7.25	49.58	0.20	42.31	0.66
2	32.99	39.44	0.00	27.40	0.18
3	25.09	53.21	0.00	21.69	0.00
4	5.23	30.36	0.00	63.58	0.83
5	4.85	5.00	0.08	87.77	2.30
Mean value	15.08	35.52	0.06	48.55	0.80

Spectrum, Mass percent (%) Elements	C	O	Fe	Ni
1	9.52	55.69	30.01	4.78
2	4.73	57.30	33.90	4.07
3	3.99	56.71	35.43	3.87
4	13.47	53.01	29.98	3.54
5	7.69	52.88	31.78	7.71
6	9.41	10.60	70.55	9.44
Mean value	8.14	47.70	38.60	5.57

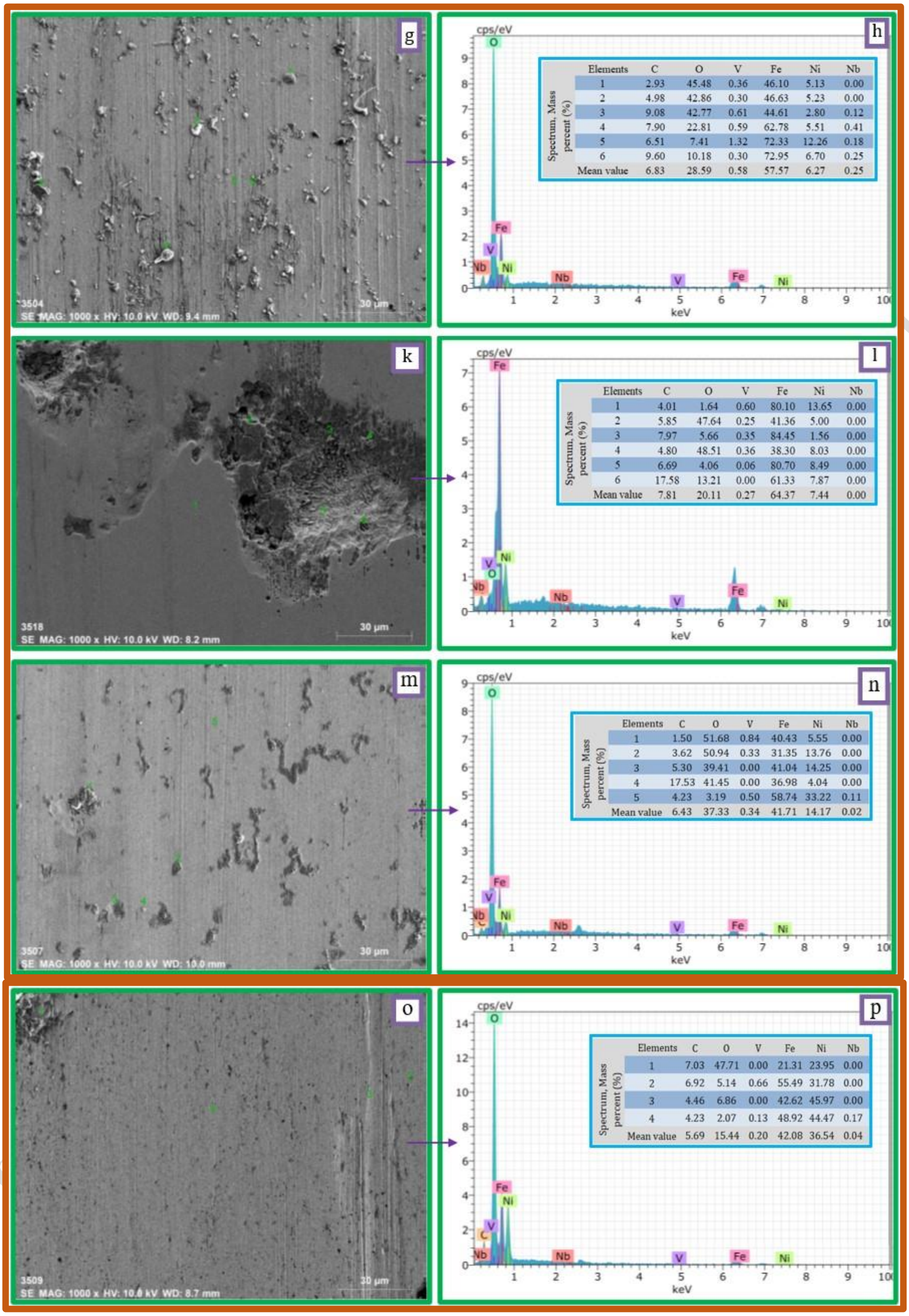
g
h
cps/eV
Elements C O V Fe Ni Nb
Spectrum, Mass percent (%)
1 2.93 45.48 0.36 46.10 5.13 0.00
2 4.98 42.86 0.30 46.63 5.23 0.00
3 9.08 42.77 0.61 44.61 2.80 0.12
4 7.90 22.81 0.59 62.78 5.51 0.41
5 6.51 7.41 1.32 72.33 12.26 0.18
6 9.60 10.18 0.30 72.95 6.70 0.25
Mean value 6.83 28.59 0.58 57.57 6.27 0.25
keV
SE MAG: 1000 x HV: 10.0 kV WD: 9.4 mm
30 μm
k
l
Elements C O V Fe Ni Nb
1 4.01 1.64 0.60 80.10 13.65 0.00
2 5.85 47.64 0.25 41.36 5.00 0.00
3 7.97 5.66 0.35 84.45 1.56 0.00
4 4.80 48.51 0.36 38.30 8.03 0.00
5 6.69 4.06 0.06 80.70 8.49 0.00
6 17.58 13.21 0.00 61.33 7.87 0.00
Mean value 7.81 20.11 0.27 64.37 7.44 0.00
SE MAG: 1000 x HV: 10.0 kV WD: 8.2 mm
m
n
Elements C O V Fe Ni Nb
1 1.50 51.68 0.84 40.43 5.55 0.00
2 3.62 50.94 0.33 31.35 13.76 0.00
3 5.30 39.41 0.00 41.04 14.25 0.00
4 17.53 41.45 0.00 36.98 4.04 0.00
5 4.23 3.19 0.50 58.74 33.22 0.11
Mean value 6.43 37.33 0.34 41.71 14.17 0.02
SE MAG: 1000 x HV: 10.0 kV WD: 10.0 mm
o
p
Elements C O V Fe Ni Nb
1 7.03 47.71 0.00 21.31 23.95 0.00
2 6.92 5.14 0.66 55.49 31.78 0.00
3 4.46 6.86 0.00 42.62 45.97 0.00
4 4.23 2.07 0.13 48.92 44.47 0.17
Mean value 5.69 15.44 0.20 42.08 36.54 0.04
SE MAG: 1000 x HV: 10.0 kV WD: 8.7 mm

Figure 6.

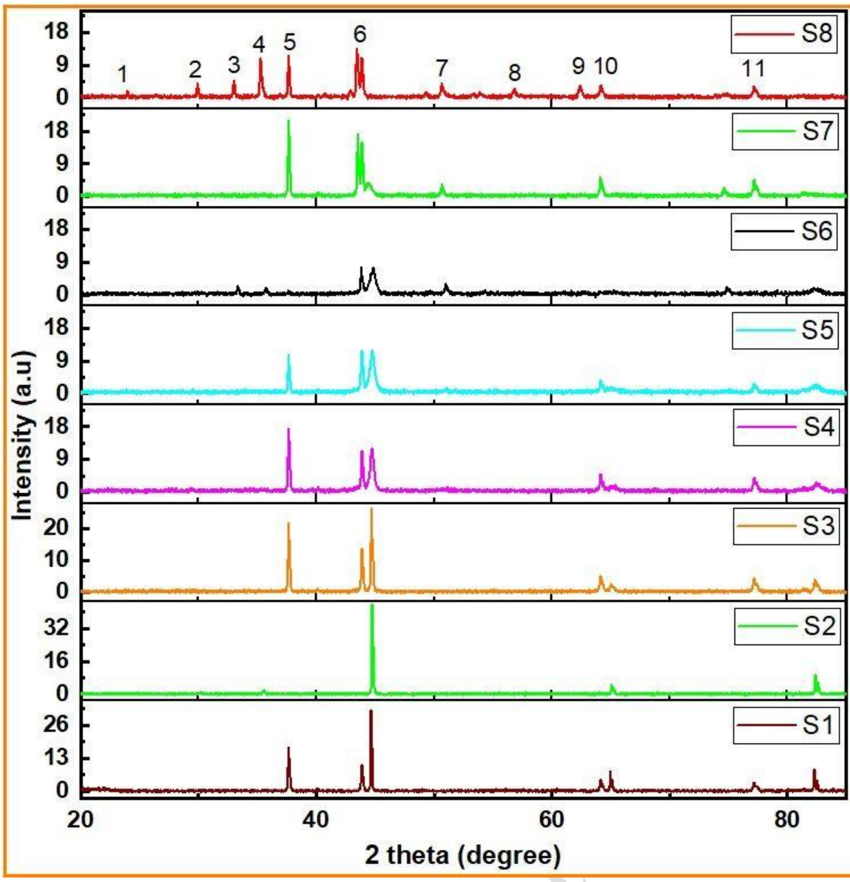

Formula	Pik Number
Fe	6, 7, 11
Fe, C	6, 7, 11
Fe_2C	5, 6, 8
Fe_3C	4, 5, 6, 7, 8, 9, 10, 11
Fe_5C_2	4, 5, 6, 7, 8, 11
Fe, Nb	4, 5, 6, 11
Fe_2Nb	2, 5, 6, 7, 8, 9, 11
Fe_2Nb_3	4, 5, 6
FeNi	6,7, 8, 11
Fe, Ni	2, 3, 4, 6,7, 8 11
$FeNi_3$	6,7, 11
Fe_3Ni_2	6, 7, 11
FeV	6, 10, 11
C	6, 11
C_{60}	1, 2, 3, 5, 6, 7
$C_{0.63}Fe_4$	6, 11
C_3Fe_7	6, 10, 11
C_5V_6	5, 6, 9, 11
VC	5, 6, 7, 9, 11
VCN	4, 6, 7, 10, 11
$VC_{0.75}$	5, 6, 10, 11
V_8C_7	5, 6, 9, 11
VFe	6, 10
V_3Fe_2	6, 10
NbC	4, 6, 10, 11
NbN	4, 6, 7, 10, 11
NbCN	4, 6, 7, 10, 11
Ni, Fe	6, 7, 11
Ni_2V	6, 7, 11
Ni_3V	6, 7, 11
Ni_8Nb	4, 5, 6, 7, 8, 11

Figure 7.

<table>
<tr><th>Samples</th><th>Dry Wear</th><th>Corrosion Wear</th></tr>
<tr><td>S1</td><td>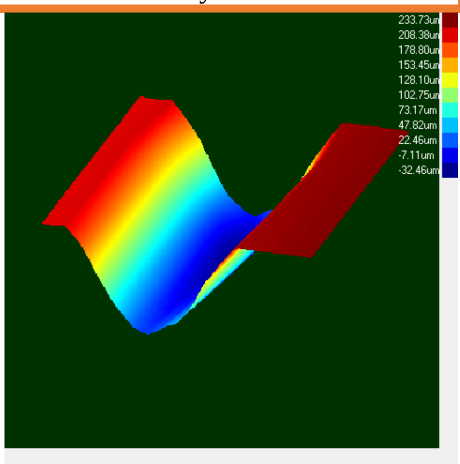
</td><td>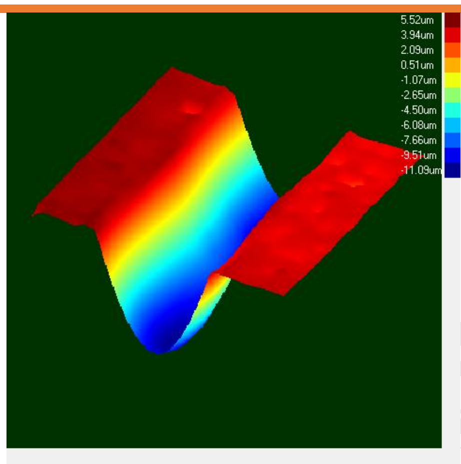
</td></tr>
<tr><td>S2</td><td>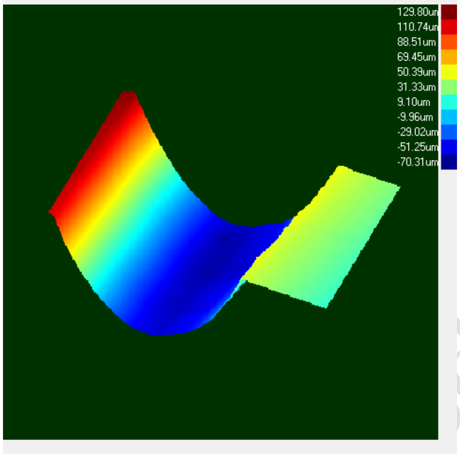
</td><td>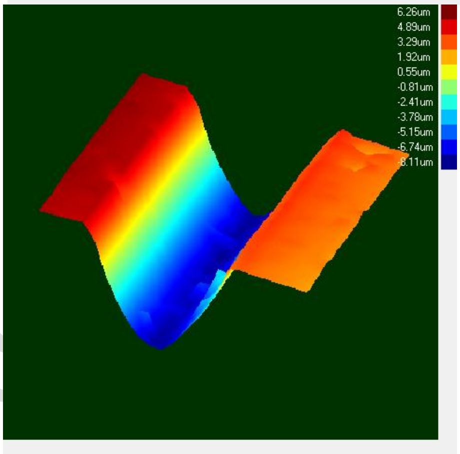
</td></tr>
<tr><td>S3</td><td>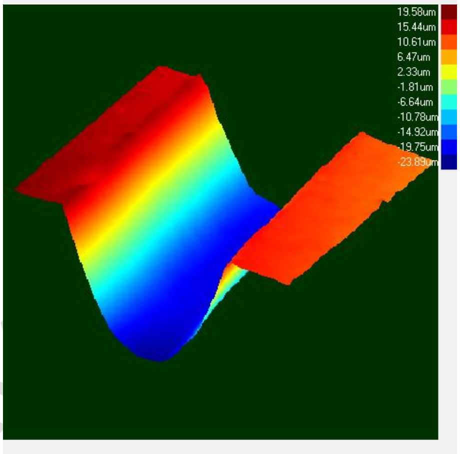
</td><td>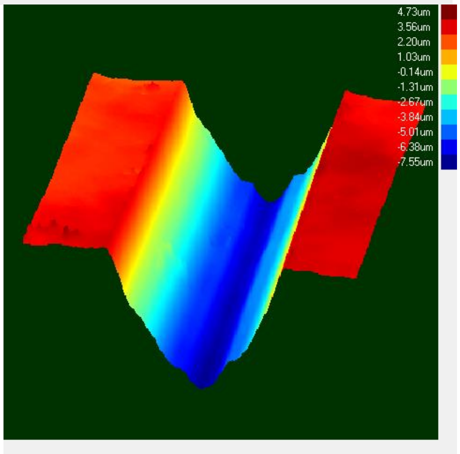
</td></tr>
</table>

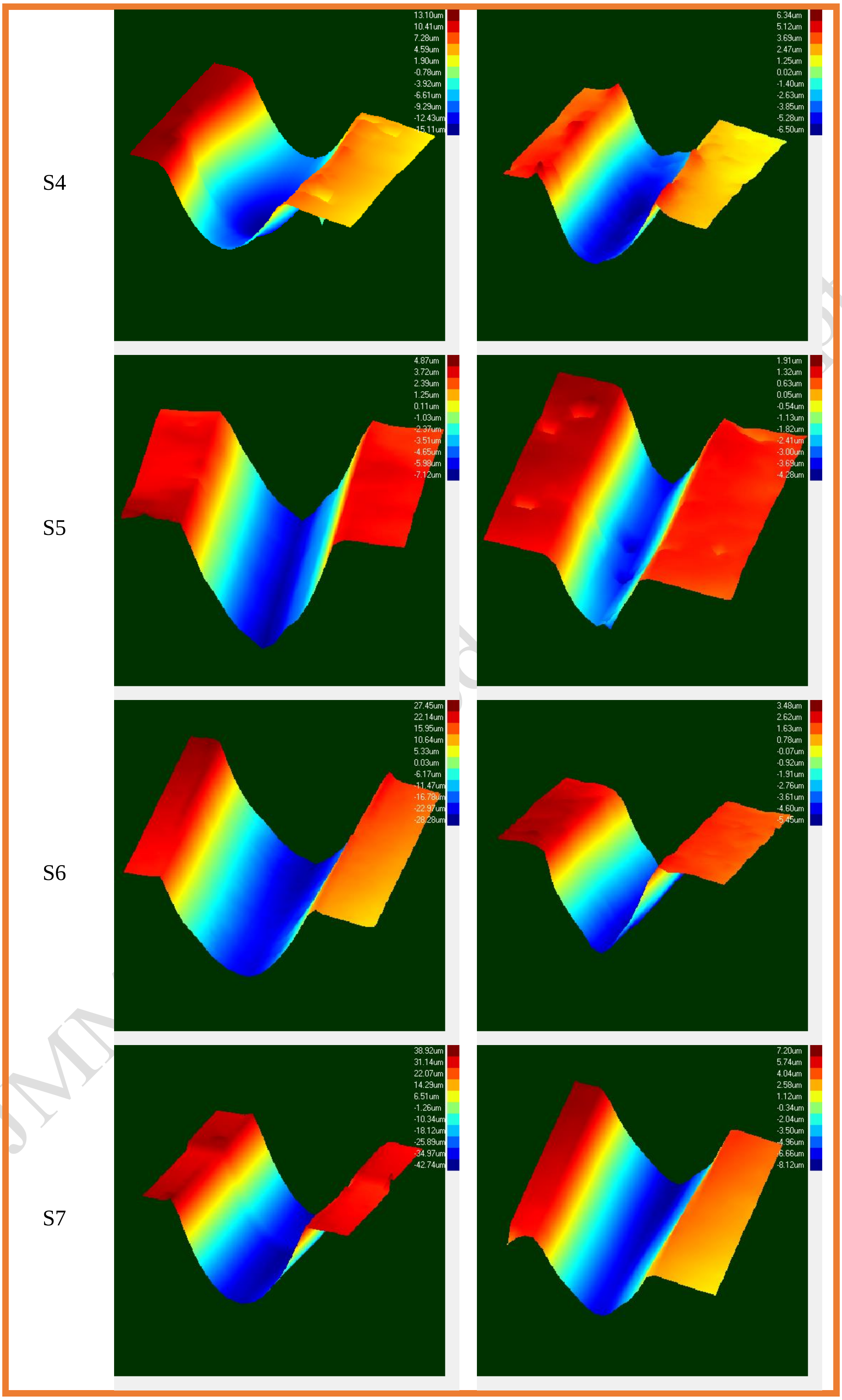
S4
13.10um
10.41um
7.28um
4.59um
1.90um
-0.78um
-3.92um
-6.61um
-9.29um
-12.43um
-15.11um
6.34um
5.12um
3.69um
2.47um
1.25um
0.02um
-1.40um
-2.63um
-3.85um
-5.28um
-6.50um
S5
4.87um
3.72um
2.39um
1.25um
0.11um
-1.03um
-2.37um
-3.51um
-4.65um
-5.98um
-7.12um
1.91um
1.32um
0.63um
0.05um
-0.54um
-1.13um
-1.82um
-2.41um
-3.00um
-3.69um
-4.28um
S6
27.45um
22.14um
15.95um
10.64um
5.33um
0.03um
-6.17um
-11.47um
-16.78um
-22.97um
-28.28um
3.48um
2.62um
1.63um
0.78um
-0.07um
-0.92um
-1.91um
-2.76um
-3.61um
-4.60um
-5.45um
S7
38.92um
31.14um
22.07um
14.29um
6.51um
-1.26um
-10.34um
-18.12um
-25.89um
-34.97um
-42.74um
7.20um
5.74um
4.04um
2.58um
1.12um
-0.34um
-2.04um
-3.50um
-4.96um
-6.66um
-8.12um

S8

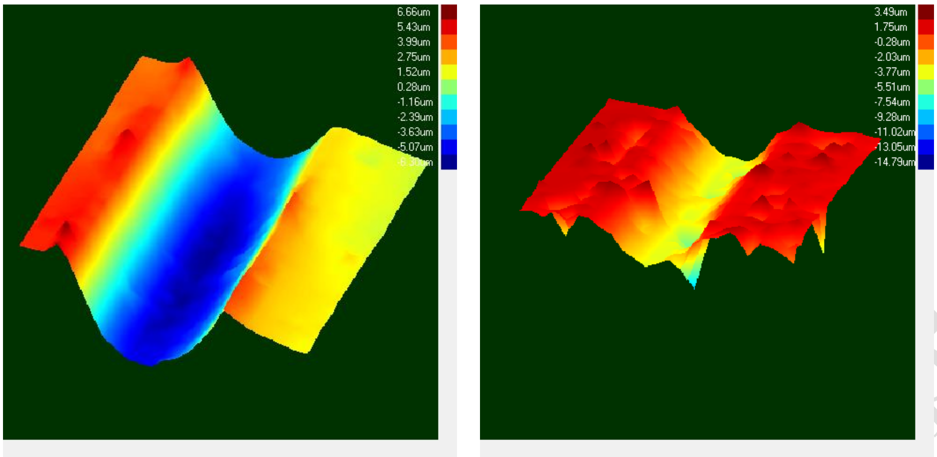

6.66um
5.43um
3.99um
2.75um
1.52um
0.28um
-1.16um
-2.39um
-3.63um
-5.07um
-6.30um
3.49um
1.75um
-0.28um
-2.03um
-3.77um
-5.51um
-7.54um
-9.28um
-11.02um
-13.05um
-14.79um

Figure 8.

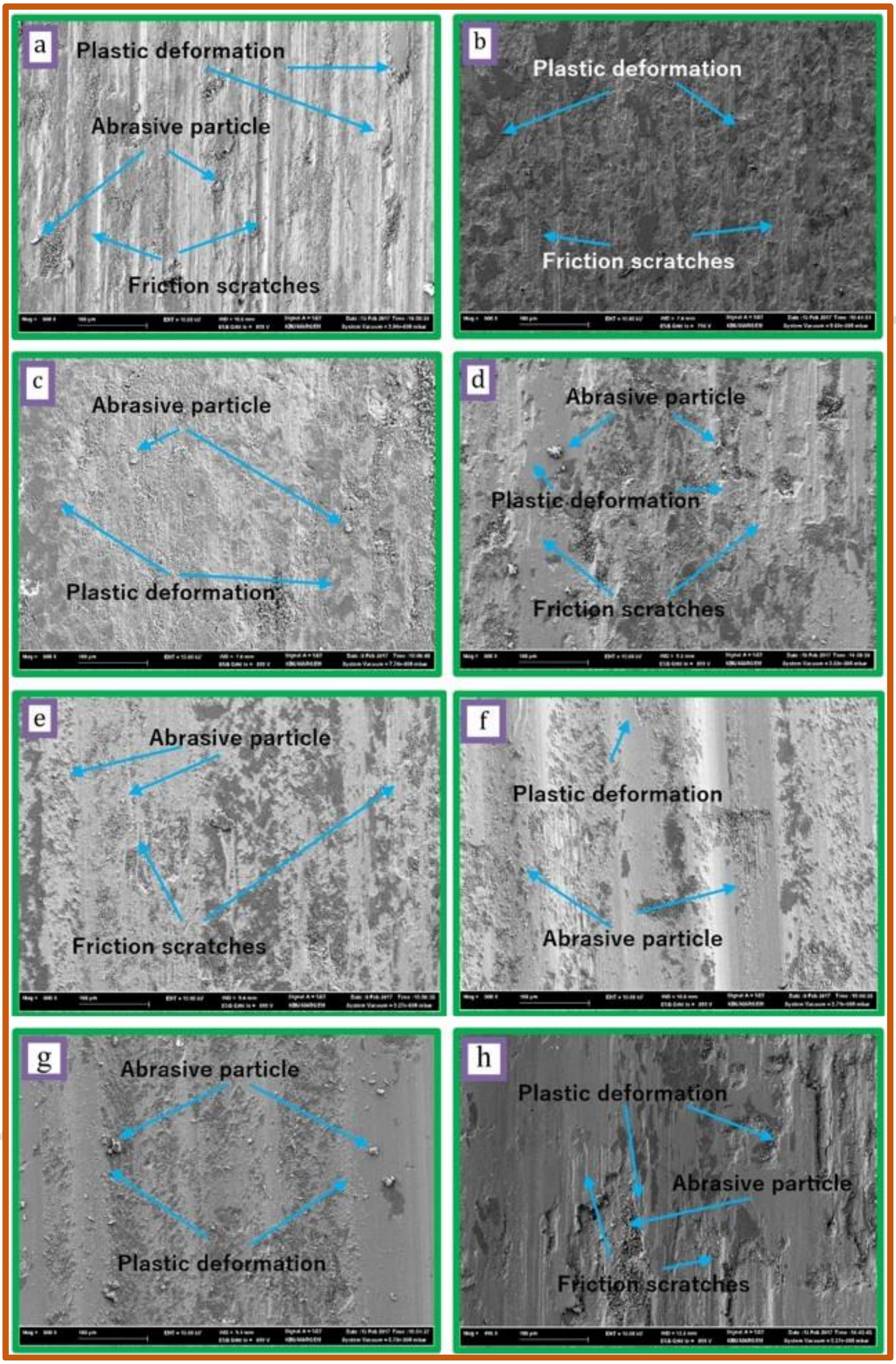

a
Plastic deformation
Abrasive particle
Friction scratches
b
Plastic deformation
Friction scratches
c
Abrasive particle
Plastic deformation
d
Abrasive particle
Plastic deformation
Friction scratches
e
Abrasive particle
Friction scratches
f
Plastic deformation
Abrasive particle
g
Abrasive particle
Plastic deformation
h
Plastic deformation
Abrasive particle
Friction scratches

Figure 9.

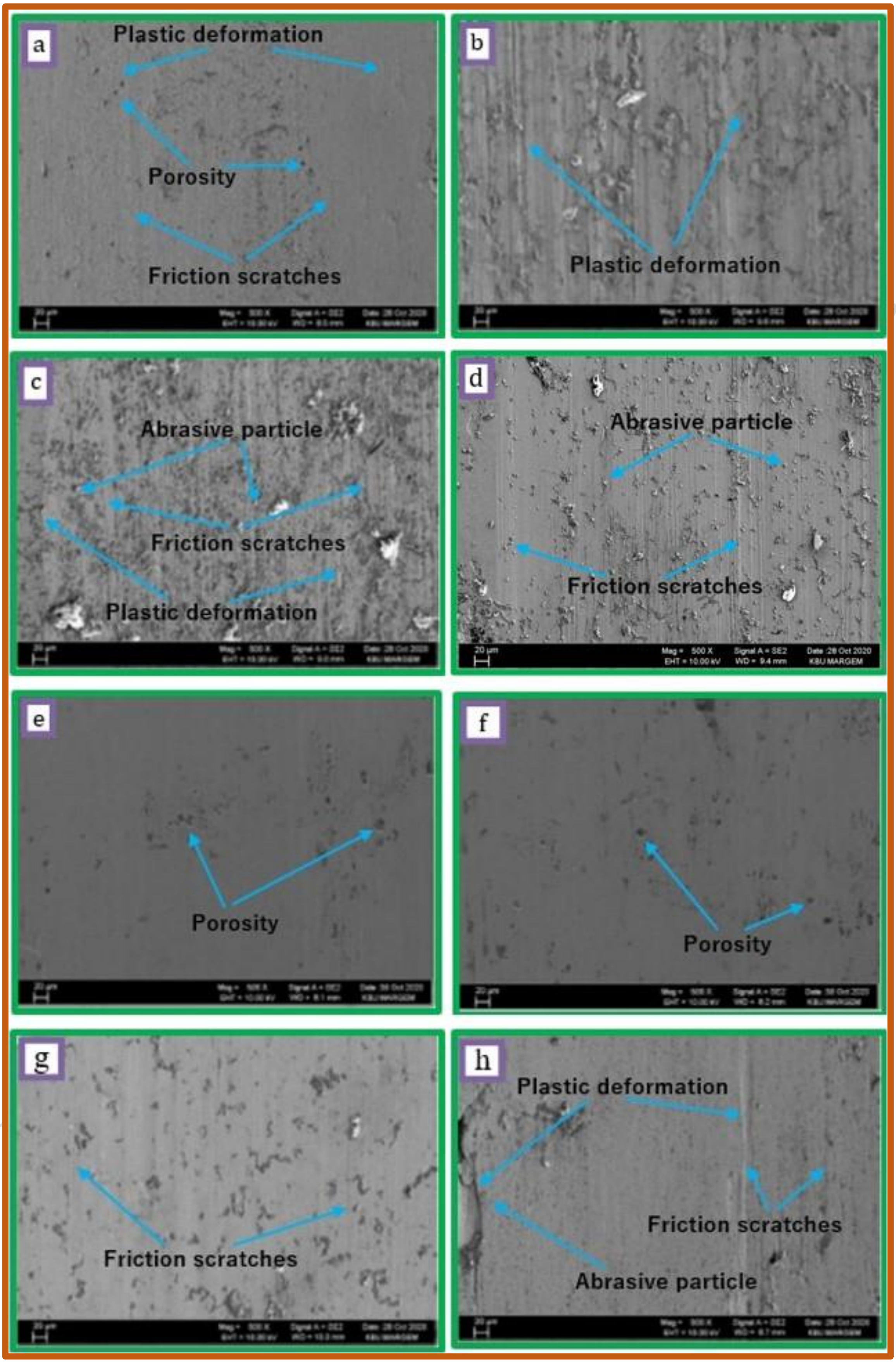

a
Plastic deformation
Porosity
Friction scratches
b
Plastic deformation
c
Abrasive particle
Friction scratches
Plastic deformation
d
Abrasive particle
Friction scratches
e
Porosity
f
Porosity
g
Friction scratches
h
Plastic deformation
Friction scratches
Abrasive particle

Figure 10.

Table List

Table 1.

Samples	Compound	Mass spectrum (% wt)				
		Graphite	Nb	V	Ni	Fe
S1	Fe + C	0.55	-	-	-	rest
S2	Fe + C + 0.15 (Nb + V)	0.55	0.075	0.075	-	rest
S3	Fe + C + 0,15 (Nb + V) + 5Ni	0.55	0.075	0.075	5	rest
S4	Fe + C + 0.15 (Nb + V) + 10Ni	0.55	0.075	0.075	10	rest
S5	Fe + C + 0.15 (Nb + V) + 13Ni	0.55	0.075	0.075	13	rest
S6	Fe + C + 0.15 (Nb + V) + 15Ni	0.55	0.075	0.075	15	rest
S7	Fe + C + 0.15 (Nb + V) + 20Ni	0.55	0.075	0.075	20	rest
S8	Fe + C + 0.15 (Nb + V) + 30Ni	0.55	0.075	0.075	30	rest

Table 2.

Samples	Load in dry sliding (N)				Load in corrosive sliding (N)				Density (g/cm3) [55]	Hardness ($HV_{0.5}$) [55]
	15		30		15		30			
	Wear loss (mg)	Friction coefficient	Wear loss (mg)	Friction coefficient	Wear loss (mg)	Friction coefficient	Wear loss (mg)	Friction coefficient		
S1	24.255	0.0968	35.866	0.0980	3.568	0.0721	6.882	0.0649	7.2837	75
S2	13.466	0.0972	23.118	0.1086	2.776	0.0791	5.450	0.0638	7.2787	125
S3	9.430	0.0985	15.187	0.1043	2.388	0.0721	5.008	0.0898	7.4102	160
S4	4.558	0.0936	8.813	0.1098	1.504	0.0688	3.972	0.0746	7.2347	243
S5	2.734	0.1028	7.367	0.1164	1.344	0.0872	3.704	0.0897	7.5947	244
S6	3.912	0.1126	9.550	0.1187	1.596	0.0856	4.628	0.0862	7.6724	191
S7	5.908	0.1092	13.182	0.1182	2.188	0.0831	4.976	0.0844	7.6212	133
S8	8.804	0.0975	17.999	0.1019	2.608	0.0689	5.561	0.0555	7.2903	93